Int J Earth Sci (Geol Rundsch) (2017) 106:1597–1617
DOI 10.1007/s00531-016-1371-7

ORIGINAL PAPER

Mineral chemistry as a tool for understanding the petrogenesis of Cryogenian (arc-related)–Ediacaran (post-collisional) gabbros in the western Arabian Shield of Saudi Arabia

Adel A. Surour[1] · Ahmed H. Ahmed[2,3] · Hesham M. Harbi[2]

Received: 18 February 2016 / Accepted: 30 June 2016 / Published online: 9 July 2016

Abstract Metagabbros and gabbros in the Ablah-Shuwas belt (western Saudi Arabia) represent part of significant mafic magmatism in the Neoproterozoic Arabian Shield. The metagabbros are Cryogenian, occasionally stratified and bear calcic amphiboles (hornblende, magnesio-hornblende and actinolite) typical of calc-alkaline complexes. These amphiboles suggest low pressure (~1–3 kbar), high f_{O_2} and crystallization temperature up to 727 °C, whereas it is 247–275 °C in the case of retrograde chlorite. Rutile and titanite in metagabbros are Fe-rich and replace Mn-bearing ilmenite precursors at high f_{O_2}. On the other hand, younger gabbros are fresh, layered and comprised of olivine gabbro and olivine–hornblende gabbro with an uppermost layer of anorthositic gabbro. The fresh gabbros are biotite-bearing. They are characterized by secondary magnetite–orthopyroxene symplectitic intergrowth at the outer peripheries of olivine. The symplectite forms by deuteric alteration from residual pore fluids moving along olivine grain boundaries in the sub-solidus state. In fresh gabbros, ortho- and clinopyroxenes indicate crystallization at 1300–900 and 800–600 °C, respectively. Geochemically, the Cryogenian metagabbros (~850–780 Ma) are tholeiitic to calc-alkaline in composition and interpreted as arc-related. Younger, fresh gabbros are calc-alkaline and post-collisional (~620–590 Ma, i.e., Ediacaran), forming during the late stages of arc amalgamation in the southern Arabian Shield. The calc-alkaline metagabbros are related to a lithospheric mantle source previously modified by subduction. Younger, fresh gabbros were probably produced by partial melting of an enriched mantle source (e.g., garnet lherzolite).

Keywords Ablah-Shuwas · Mafic magma · Calc-alkaline · Arc-related · Symplectite · P–T estimates

Introduction

The application of mineral chemistry to understanding the petrogenesis of Neoproterozoic mafic magmatism in the Arabian Shield is completely lacking. We present the first chemical analyses of silicate and non-silicate minerals to unravel the petrogenesis associated with emplacement of Neoproterozoic gabbroic rocks in the Arabian Shield. Such mafic magmatism is recorded as two separate (Cryogenian and Ediacaran) pulses of calc-alkaline affinity based on whole-rock chemistry (e.g., Johnson et al. 2011, 2013). The Precambrian rocks of the Arabian Shield cover approximately 650,000 km^2 of the Western Arabian Peninsula. The rocks of the Arabian Shield are mostly Neoproterozoic in age, but some date from the Archean and Paleoproterozoic, and a few intrusions yield Cambrian ages (Nehlig et al. 1999, 2002). The terrane concept has been applied to the Arabian and Nubian Shields since the mid-1980s developing out of earlier plate tectonic/subduction zone and accreted island-arc concepts. The exposed and immediately adjacent concealed Proterozoic rocks of western Arabia

Electronic supplementary material The online version of this article (doi:10.1007/s00531-016-1371-7) contains supplementary material, which is available to authorized users.

✉ Adel A. Surour
adelsurour@hotmail.com

[1] Geology Department, Faculty of Science, Cairo University, Giza 12613, Egypt

[2] Department of Mineral Resources and Rocks, Faculty of Earth Sciences, King Abdulaziz University, P.O. Box 60206, Jeddah 21589, Saudi Arabia

[3] Geology Department, Faculty of Science, University of Helwan, Ain Helwan, Cairo, Egypt

and northeastern Africa are interpreted as a collage of crustal blocks or terranes that can be correlated across the Red Sea, thereby linking the now separated Arabian and Nubian Shields. The island-arcs in the Arabian–Nubian Shield represent juvenile terranes (e.g., Asir, Jeddah and Hijaz; Fig. 1) at ~900–780 Ma (Harris et al. 1990; Johnson et al. 2013). They developed by intraoceanic subduction in the Mozambique Ocean that resulted from rifting of Rodinia (Greiling et al. 1994; Abdelsalam and Stern 1996; Blasband 2006). It is generally accepted that rocks of the Arabian Shield were variously amalgamated between about 780 and 640 Ma, as indicated by the crystallization age of syn-tectonic intrusions along the sutures (Johnson et al. 2011).

Based on intensive geological, geochemical, age-dating and structural studies, several plate tectonic interpretations of the Precambrian history of the Arabian–Nubian Shield in general and the Arabian Shield in particular have been made by numerous authors. Several tectonic models for the evolution of the basement rocks in the Arabian Shield have been proposed (e.g., Gass 1981; Kröner 1985; Kemp et al. 1980, 1982; Duyverma 1984; Johnson et al. 2011, 2013). According to some models, the tectonic evolution of the shield involved four stages that started with the oldest oceanic arc system and ended by the so-called "the Najd orogeny" that might have lasted until the Cambrian (Duyverma 1984; Stern 1994). Genna et al. (2002) suggested a detailed view of the anatomy and geologic history of the Arabian Shield based on a geologic, structural, geochemical and geochronologic synthesis. The main geologic evolution of the Shield is limited to the period ranging from 900 to 530 Ma that led to the formation, amalgamation and final cratonization of several tectono-stratigraphic terranes. The majority of magmatic activity post-dating amalgamation in the Arabian Shield took place during the Ediacaran and resulted in arc and post-orogenic magmas that led to the emplacement of several phases of mafic–felsic plutons and stocks (Johnson 2006; Johnson et al. 2011, 2013).

In the Arabian–Nubian Shield, non-ophiolitic mafic–ultramafic complexes are represented by Alaskan-type gabbroic intrusions (with some ultramafics) that are concentrically zoned or layered intrusions that occur as small elliptical bodies along major structures (Helmy and El-Mahallawi 2003; Abd El-Rahman et al. 2012; Abdel Halim et al. 2016). The Alaskan-type intrusions are post-tectonic and represent uplifted fragments of the deep levels of island-arcs, particularly the back-arcs (Helmy et al. 2014, 2015). On the other hand, the layered intrusions are underformed and are almost devoid of ultramafic rocks (El-Mettwaly 1992; Azer and El Gharabawi 2011). The magma type of layered gabbroic complexes in the Arabian–Nubian

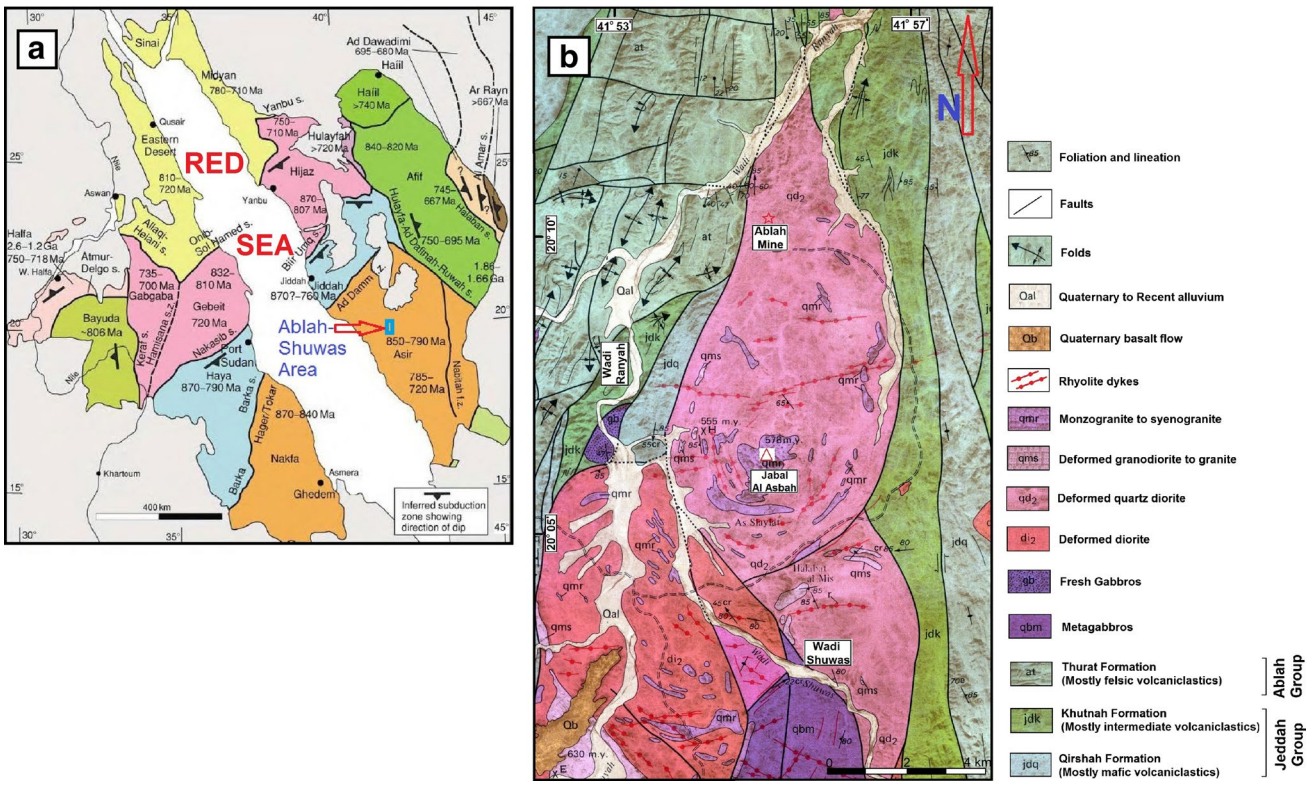

Fig. 1 **a** Location map of the Ablah-Shuwas area on the Arabian–Nubian Shield terrane map of Johnson and Woldehaimanot (2003). **b** Modified geological map of the Ablah-Shuwas area after Greenwood (1972)

Shield varies from tholeiitic through calc-alkaline to alkaline attributed by Be'eri-Shlevin et al. (2009) to coeval derivation from variable sources rather than formation in different tectonic settings.

This study presents mineralogical and geochemical data from mafic rocks in the Ablah-Shuwas area. The mineral chemistry data represent the first detailed mineralogical analyses of both metagabbros and fresh gabbros, and apply these data to estimate the prevailing temperature, pressure and oxygen fugacity upon crystallization and emplacement with respect to the tectonic framework of Neoproterozoic shield rocks in the Asir terrane (Fig. 1a). The source of this magmatism, its geochemical type and possible tectonic setting are discussed. In addition, a synopsis on the origin of symplectite intergrowths in the fresh gabbros is also presented. Whole-rock geochemistry is not the main topic of the present work, but representative analyses are given in support of the conclusions obtained from electron microprobe analyses (EMPA).

Geology of the Ablah-Shuwas area

In the Ablah area, a thick succession of Neoproterozoic rocks is present which comprise both layered (stratified) and intrusive rocks with great variations in relative age, lithology and deformation. The oldest rock unit is an ophiolitic mélange in which deformed serpentinite, metagabbro and metabasalt fragments are enclosed in chlorite and quartz–biotite schists as a low-grade matrix. Some relict fresh mantle dunite and peridotite are still preserved in the serpentinites.

The layered rocks of the Ablah-Shuwas area are represented by four volcano-sedimentary assemblages that are subdivided into the Baish, Bahah, Jeddah and Ablah Groups, from oldest to youngest. Around Jabal Ablah itself, the layered rocks are only represented by the Jeddah Group, whereas the other three groups are present outside the limits of the geological map given in Fig. 1b. The oldest groups (Baish and Bahah) consist of metabasalt, mafic to intermediate metatuffs, chlorite schist, garnet quartzite and weakly metamorphosed arkose, chert, graywacke and graphitic wacke. The Jeddah Group is subdivided into the basal Qirshah Formation (metaandesite–dacite and minor marble) and the upper Khutnah Formation (metavolcaniclastics, thick marble and metaconglomerate). The Ablah Group was subdivided by Greenwood (1972) from base to top into the Rafa Formation (arkosic wacke, plymictic conglomerate and foliated syn-Ablah diorite and quartz diorite intrusions), the Jerub Formation (metaandesite–latite, rhyolite flows and sills and flow breccias) and the Thurat Formation (stramatolitic marble, rhyolite, andesite and volcanic wackes). According to Greenwood (1972) and Hadley and Fleck (1980), the four volcano-sedimentary groups were weakly metamorphosed under greenschist facies conditions and amphibolite hornfels facies are only reported in the thermal aureoles induced by the younger intrusive rocks. Regional metamorphism increases southwards to amphibolite facies as in Wadi Baysh located south of the Ablah area (Farier 1985).

The tectono-stratigraphy of the Ablah area has received a lot of attention since the first notes of Zakir (1972). Bamousa (2013) and Hamimi et al. (2014) pointed out the complexity of folding and schistosity representing at least three deformational phases (D1, D2 and D3). One of the prominent structural features is the development of N–S trending brittle–ductile shear zone(s) in the Asir Terrane which may be contemporaneous with D2 folding and late Neoproterozoic syn-tectonic intrusions (Hamimi et al. 2013). These workers agreed with Johnson (2003) that they represent a transpressional regime possibly reflecting progressive convergence between East and West Gondwana. From a tectonic point of view, the Baish, Bahah and Jeddah Groups represent proper volcanic-arc terranes, whereas the youngest Ablah Group (Jerub Fm) developed after collision and the formation of the so-called "Ablah Graben," one of the famous intercontinental or intramontane molasses basins in the Arabian–Nubian Shield (Genna et al. 1999, 2002; Johnson 2003; Johnson et al. 2011, 2013). This timing was contemporaneous with the East African Orogen (EAO) about 640–615 Ma ago (Stern 1994; Stern and Johnson 2010). The molasse-type volcano-sedimentary assemblage or post-amalgamation basin rocks of the Ablah Group formed in a N–S trending basin in a marine environment, whereas its counterparts further north in the Arabian–Nubian Shield form as mixed terrestrial-shallow marine assemblages (Johnson et al. 2011). Based on structural analyses, Hamimi et al. (2014) believed that the Ablah Group was deposited in a strike-slip pull-apart basin that developed during or soon after the so-called Nabitah Orogen (680–640 Ma), which was almost contemporaneous with the EAO of Stern (1994). Precise SHRIMP zircon dating of rhyolite interbedded with sandstone–siltstone–mudstone–dolostone of the upper Ablah epiclastic unit suggests an age of 613 ± 7 Ma (Johnson et al. 2001). Recently, detailed lithostratigraphic and microscopic investigations suggest stromatolitic carbonates may have formed in the upper Ablah epiclastic unit when volcanism paused, followed by syn-sedimentary and diagenetic alteration of mafic tuffs (Taj and Mesaed 2011). The youngest terrane amalgamation event reported in the Arabian–Nubian Shield took place 620 ± 3 Ma ago and is only preserved in the eastern extreme of the Arabian Shield (Cox et al. 2012).

The oldest intrusive rocks in the Ablah area are represented by the pre-Ablah quartz diorite–metagabbro complex (895–835 Ma) at Wadi Khadrah (outside Fig. 1b),

which may be equivalent to the metadiorite complex at Wadi Sa'diyah (Wier and Hadley 1975; Fleck et al. 1980). This might represent the syn-orogenic tholeiitic to calc-alkaline magmatism contemporaneous with island-arc and microcontinent accretion between ~850 and 620 Ma in the early Cryogenian–Ediacaran (Fritz et al. 2013). Younger intrusive rocks comprise granitoids (within-plate A-type granites) and fresh layered gabbros of the Ablah-Shuwas area, which formed in the late Cryogenian–Ediacaran (~640–540 Ma) and represent post-collisional mafic–felsic magmatism of the type widespread in the Arabian–Nubian Shield (Johnson 2006). Moufti (2001) determined whole-rock Rb/Sr ages of 617 ± 17 and 605 ± 5 Ma for syenite and quartz syenite–granite, the most common A-type granitoids of the Ablah-Shuwas area and an age of 744 ± 22 Ma for the older arc-related tonalite–diorite.

Field relationships and sampling

In the Ablah-Shuwas area, gabbroic rocks are abundant and display features useful for their classification. The oldest gabbro in the area is ophiolitic and occurs as rootless intrusions or fragments in low-grade schist associate with serpentinite. The ophiolitic mafic–ultramafic association commonly decorates suture zones in the Arabian Shield of Saudi Arabia but occurs outside the study area shown in Fig. 1b, and is not the subject of this study. Our investigation focusses on the non-ophiolitic metagabbros and younger fresh gabbros of the Ablah-Shuwas area. Our observations in the Ablah-Shuwas area reveal that ophiolitic metagabbros are intruded by non-ophiolitic metagabbros and younger fresh gabbros, in addition to a wide variety of A-type granitoids represented mostly by monzogranite, syenogranite and syenite. Regionally metamorphosed gabbros must pre-date unmetamorphosed fresh gabbros; hence, metagabbros is distinguished from the younger fresh gabbros. Based on lithostratigraphy and petrology the intrusive rocks in the Ablah-Shuwas area can be classified into (1) metagabbro diorite, (2) the Shuwas pluton comprising undifferentiated quartz diorite, granodiorite and tonalite, (3) fresh gabbros and A-type granites, and finally (4) dyke rocks that are mostly rhyolite. Non-ophiolitic metagabbros occur as small intrusions particularly on the eastern flank of Wadi Raniyah (northern intrusions) and as much larger body (southern intrusion) to the south of Wadi Shuwas (Fig. 1b). The metagabbros (especially those of the northern intrusions) are occasionally layered and grade into undifferentiated pocket-like masses of metadiorite. The northern metagabbro exposures are scattered unevenly and unmappable in most of cases. They are found either as isolated masses surrounded by wadi alluvium in highly eroded parts of the Shuwas pluton or occasionally as xenoliths in the quartz diorite and granodiorite. The metagabbros are medium to coarse grained and intrude the thick volcano-sedimentary succession of the Jeddah Group. Occasionally, diffuse contacts are observed. The metagabbros themselves are intruded by pink monzo- and syenogranites (Fig. 2a), and the gabbroic rocks occur as roof pendants. On the other hand, the diorites and quartz diorites of the Shuwas pluton form sub-rounded elongated nearly N–S trending bodies generally parallel to the structures of the area. Similar to the metagabbros, the quartz diorites of the Shuwas pluton

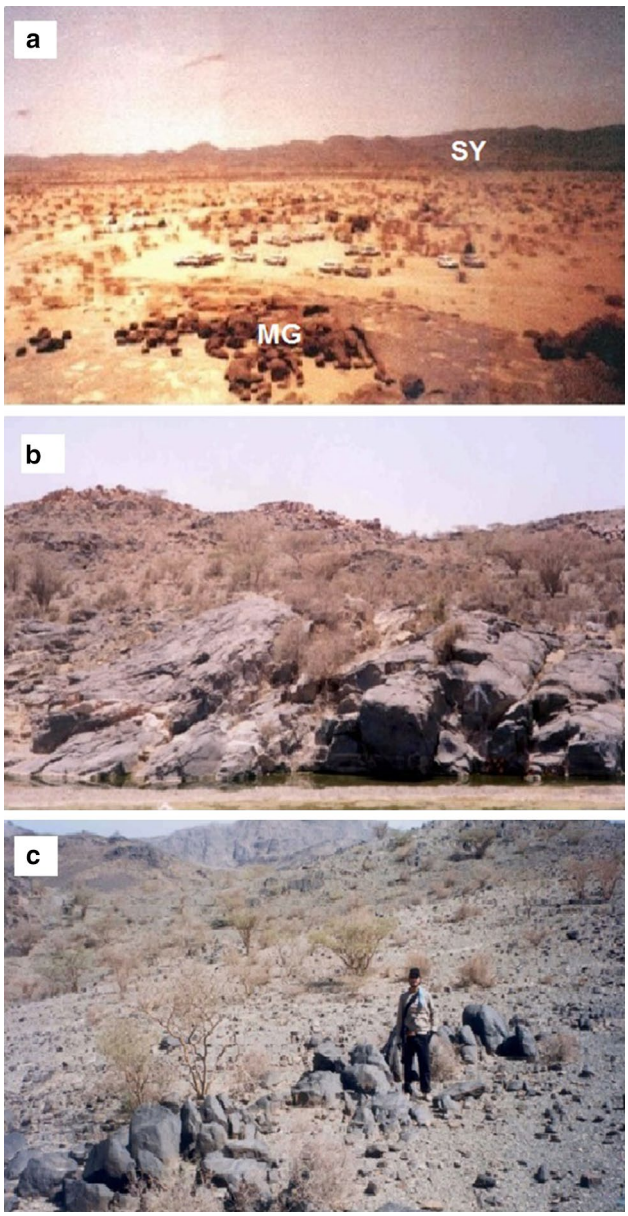

Fig. 2 **a** Northern metagabbros (*MG*), occasionally microdiorite and syenite (*SY*) in the background. Photograph looking N. **b** Major outcrop of fresh gabbros at the Wadi Raniyah, locally layered and anorthositic gabbro at the top. Photograph looking NE. **c** Bouldery weathering of the fresh olivine gabbros. Photograph looking NW

have an intrusive contact against the weakly metamorphosed volcano-sedimentary strata of the Jeddah Group. The younger fresh gabbros crop out at Wadi Raniyah near its junction with Wadi Shuwas (Fig. 1b). The fresh gabbros define a nearly oval-shaped or lobe-like body (Fig. 2b). This body is layered with light metagabbro and anorthositic gabbros at the top. At the base, troctolitic gabbro with a knobby surface is the most common variety and grades upward into olivine gabbro. The layered fresh gabbro is tilted and its average dip is 35° due NE, striking NW–SE. All fresh gabbros show bouldery weathering (Fig. 2c).

Syenogranite is the most common A-type granitoid in the area of study, and it is medium to coarse grained with a characteristic pink to yellowish pink appearance. Generally massive and underformed, it is intensively weathered at outcrops characterized by exfoliation and joints. It occurs as irregular bodies and ring-like dykes intruding the diorites and quartz diorites of the Shuwas pluton. The contact between syenite and diorite is sharp with no visible contact effects and hence a complete absence of any thermal aureole. Xenoliths and roof pendants of diorite and gabbros are present in the syenites and granites. Numerous porphyritic dacite, rhyolite and aplite dykes traverse the Shuwas pluton and the relatively older metagabbros. The northern mass of A-type granite (Fig. 1b) contains several pegmatite dykes, quartz and fluorite veins with occasional visible greisenization.

We collected a total of 23 samples for petrographic and geochemical analysis. This included 12 samples of older metagabbro from the Khutnah Formation (Jeddah Group), six from the east side of Wadi Raniyah west of Jebel Ablah (sample numbers 11a, 11b, 11c, 11d, 12a, 12b, 12c) and six from the southern part of the study area (sample numbers 6a, 6b, 6c, 66a, 66b, 66c, 66d). Nine samples of younger gabbro representing the Thurat Formation (Ablah Group) were collected south of Wadi Shuwas (sample numbers 9a, 9b, 9c, 10a, 10b, 10c, 99a, 99b, 99c).

Petrography

Metagabbro

The metagabbro shows variation in granularity (to rarely pegmatitic) and color index (mesocratic to melanocratic). There are no distinct mineralogical or textural differences between northern and southern metagabbros. In both intrusions, the rock essentially consists of plagioclase, hornblende and up to ~3 % apatite and 5–7 % Fe–Ti oxides where the later occur as intercumulus phases. Plagioclase is extensively altered to zoisite and sericite, and the relict crystals are highly corroded by hornblende (Fig. 3a). The hornblende crystals are coarse, occurring as patches and they grades into actinolitic hornblende lathes at the outer peripheries (Fig. 3b). Coarse apatite is common (Fig. 3c). Opaques (Fig. 4a–e) are represented mostly by Fe–Ti oxides and much lesser oxidized pyrite. Homogenous magnetite and ilmenite are common and they are present with nearly equal amounts with ilmenite–magnetite exsolution intergrowth. The homogeneous and exsolved magnetite shows very limited martitization and ilmenite is severely altered to rutile–hematite sub-graphic intergrowth. Sometimes, fine hematite blebs are exsolved in ilmenite to form a very characteristic hemoilmenite intergrowth. Pyrite shows rim replacement by colloform goethite, and a few fresh pyrites are enclosed by homogeneous magnetite.

Fresh olivine gabbro

Olivine gabbro is coarse grained and consists of plagioclase, pyroxene, olivine, biotite and brown hornblende. Accessory minerals are represented by apatite and opaque minerals, whereas secondary minerals are chlorite, sericite, serpentine and iddingsite. Olivine is often fresh, rounded to sub-rounded with common iddingsite alteration along cracks. Plagioclase occurs as coarse crystals with well-developed pericline twining. Fine apatite needles occur as mineral inclusions in plagioclase. Clinopyroxene totally or partially encloses feldspar forming very prominent ophitic and sub-ophitic textures (Fig. 3d). In some instances, diopside rims olivine forming corona-like textures (Fig. 3e). Hornblende is a brown variety that occurs exclusively as an interstitial phase. Similarly, biotite is interstitial or partly rimming olivine and Fe–Ti oxides (Fig. 3f). Clinopyroxene is fresh diopside, whereas orthopyroxene (mostly enstatite) forms symplectite intergrowth along olivine crystal boundaries (Fig. 3g, h). The total opaque percentage reaches up to 8 % and they are represented by fresh sulfides in the form of exsolution intergrowths in which pyrrhotite is always the host mineral. Either homogeneous or intergrowths of magnetite and ilmenite are also observed (Fig. 4f). Sulfides represent ~40 % of the total opaques and they are represented by exsolved chalcopyrite in pyrrhotite or more frequently in the form of homogeneous pyrrhotite and pyrite (Fig. 4g, h).

Fresh hornblende gabbro

Generally, the rock is coarse-grained and consists mainly of hornblende- and plagioclase-rich, with lesser amounts of olivine and pyroxene. Accessory and alteration minerals are apatite, zoisite and chlorite. Appreciable amount of Fe–Ti oxides up to ~7 % characterizes this gabbroic variety. Hornblende includes resorbed plagioclase and usually corrodes pyroxene and sometimes occurs as inclusions in plagioclase. Some hornblende is altered to chlorite.

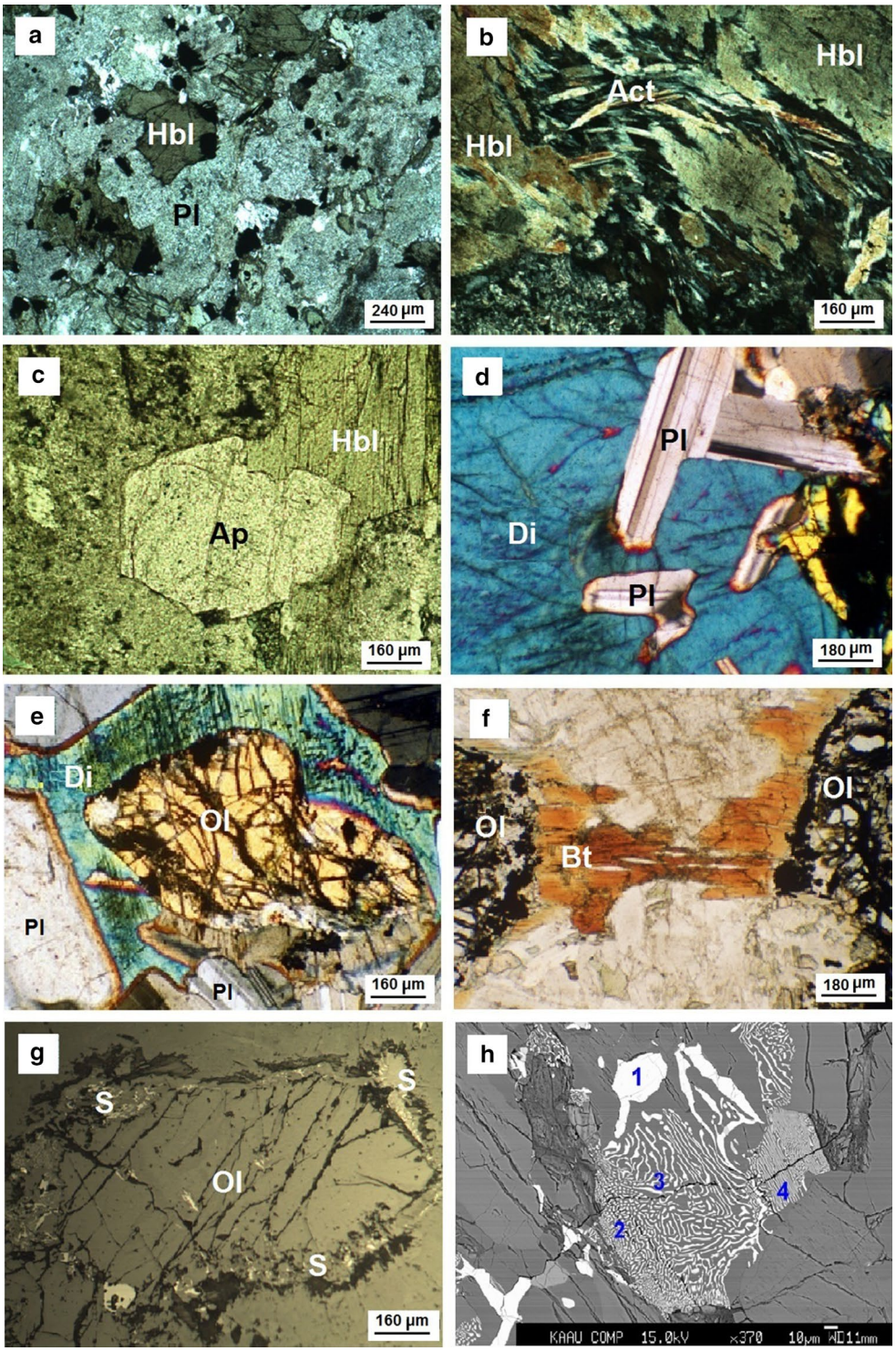

Fig. 3 Petrographic characteristics of the gabbroic rocks. *P.P.L.* plane-polarized light and *C.N.* cross-nicols. **a** General view of northern metagabbros showing extensively altered plagioclase (*Pl*) and anhedral patches of hornblende (*Hbl*), P.P.L. **b** Hornblende (*Hbl*) grades into peripheral actinolite (*Act*) in the northern metagabbros, C.N. **c** Apatite (*Ap*) is partly enclosed by hornblende (*Hbl*) in the northern metagabbros, P.P.L. **d** Diopside (*Di*) and fresh plagioclase (*Pl*) forming ophitic and sub-ophitic textures in fresh olivine gabbro, C.N. **e** Interstitial diopside (*Di*) to plagioclase (*Pl*) forming corona-like texture with olivine (*Ol*) in fresh olivine gabbro, C.N. **f** Interstitial biotite (*Bt*) and altered olivine (*Ol*) in fresh anorthositic gabbro, C.N. **g** Formation of symplectite (*S*) at the peripheral zone of olivine (*Ol*), polarized reflected light. **h** Back-scattered electron (*BSE*) image showing different types of symplectite fabrics: *1* coarse and irregular, *2* bleb-like, *3* vermicular and *4* linear

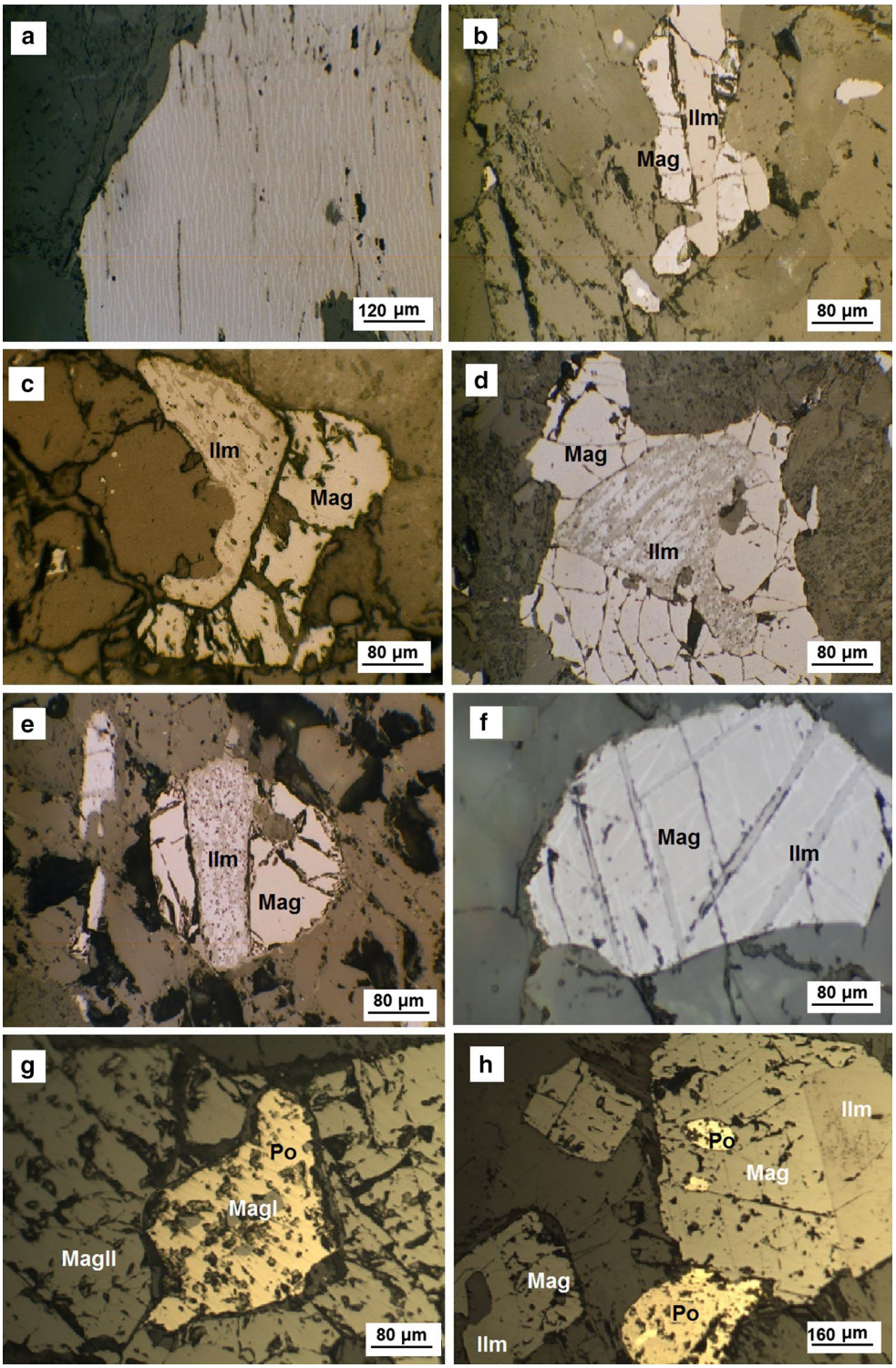

Fig. 4 Ore minerals and their fabrics the gabbroic rocks. All microphotographs are in polarized reflected light. **a** Hematite (fine, light)-ilmenite (dark host) exsolution intergrowth in the northern metagabbros. **b** Banded ilmenite (*Ilm*)–magnetite (*Mag*) intergrowth in the northern metagabbros. **c** Composite ilmenite (*Ilm*)–magnetite (*Mag*) intergrowth in the southern metagabbros. **d** Internal granule ilmenite (*Ilm*)–magnetite (*Mag*) intergrowth in the southern metagabbros. **e** Sandwich-type ilmenite (*Ilm*)–magnetite (*Mag*) intergrowth in the southern metagabbros. Note the freshness of magnetite and alteration of ilmenite to rutile which is the case of the previous four microphotographs too. **f** Ilmenite (*Ilm*)–magnetite (*Mag*) network to fine trellis in the fresh olivine gabbros. **g** Pyrrhotite (*Po*) enclosing early phase of magnetite (*MagI*) and all are hosted by much coarser magnetite (*MagII*). **h** Pyrrhotite (*Po*) inside, and adjacent to, ilmenite (*Ilm*)–magnetite (*Mag*) composite crystal with a linear contact between the two oxides

Plagioclase shows large crystals that are almost fresh with slight corrosion by hornblende. Some plagioclase is altered to sericite at the core and this may indicate a Ca-rich core. Diabasic texture is common and interstitial brown amphibole is ~45 % of the total ferromagnesian minerals. Fe–Ti oxide minerals and their fabrics are almost identical to those encountered in the fresh olivine gabbro. At the top of the section, fresh gabbro grades into thin layers and anorthositic gabbro in which oriented calcic plagioclase is dominates over mafic minerals.

Analytical methods

Major and trace element compositions of the gabbroic samples were analyzed at ACME Analytical Laboratories Ltd., Canada. Major elements, Sc, Ba and Ni concentrations were determined by inductively coupled plasma–atomic emission spectrometry (ICP-AES) after fusing 0.2 g of sample powder using $LiBO_2$. Other trace elements including REE were determined by inductively coupled plasma–mass spectrometry (ICP-MS). The geographic coordinates of samples are given in Table 1 (in addition to supplementary data, Appendix 1). Microprobe mineral analyses (supplementary data, Appendices 2 and 3) were carried out using a Jeol JXA8200 electron microprobe at the Faculty of Earth Sciences, King Abdulaziz University, Jeddah, Saudi Arabia. Electron beam conditions were 15 keV accelerating voltage, 20 nA probe current, 3 μm beam diameter and 20 s counting time for each element. The results were corrected by the ZAF method. Ferric and ferrous iron of amphibole was estimated stoichiometrically following the method of Gualda and Vlach (2005). The analyses were performed using different standards; ferro-hornblende for Si and Al; eskolaite for Cr (99.99 wt% Cr_2O_3); periclase for Mg; wollastonite for Ca; fayalite for Fe; nickel oxide for Ni (99.99 wt% NiO); $KTiPO_5$ for K and Ti; jadeite for Na; and manganosite for Mn. In few cases, quartz and corundum are used as standards for Si and Al, respectively.

Table 1 Geographic coordinates of the analyzed samples given in Table 2

Rock variety	Sample no.	Geographic coordinates
Anorthositic olivine gabbro	10 A	20°03′15″N, 41°52′55″E
	10 B	20°03′22″N, 41°53′00″E
	10 C	20°03′45″N, 41°52′57″E
Olivine gabbro	9 A	20°03′39″N, 41°52′47″E
	9 B	20°02′47″N, 41°53′00″E
	9 C	20°02′55″N, 41°53′02″E
	99 A	20°03′15″N, 41°52′55″E
	99 B	20°02′49″N, 41°52′47″E
	99 C	20°03′44″N, 41°52′57″E
Northern metagabbro	11 A	20°10′13″N, 41°56′42″E
	11 B	20°10′27″N, 41°55′15″E
	11 C	20°07′45″N, 41°56′17″E
	11 D	20°04′57″N, 41°56′00″E
	12 A	20°09′09″N, 41°56′39″E
	12 B	20°09′00″N, 41°55′31″E
	12 C	20°05′57″N, 41°55′47″E
Southern metagabbro	6 A	20°00′17″N, 41°55′39″E
	6 B	20°00′37″N, 41°55′57″E
	6 C	20°00′49″N, 41°56′17″E
	66 A	20°01′47″N, 41°56′07″E
	66 B	20°01′39″N, 41°56′08″E
	66 C	20°01′57″N, 41°55′50″E
	66 D	20°00′49″N, 41°55′55″E

Whole-rock geochemistry

Average whole-rock geochemistry is presented in Table 2 and Figs. 5, 6 and 7. The geochemical results from each unit were averaged (see supplementary material, Appendix 1). We used two averages each for the metagabbros (sample No. 6, 11, 12, 66) and fresh gabbros (sample No. 9. 10. 99). In case of fresh gabbros, the range of olivine gabbros is given when the samples of the two show variable proportions of olivine and symplectite intergrowth. From these 23 samples, 17 samples were selected for the electron microprobe mineral analysis (see supplementary material, Appendices 2 and 3) based on mineralogical variations and degree of freshness.

The gabbroic nature of all analyzed samples, either metamorphosed or fresh, is clearly shown in Fig. 5a using the adopted classification of plutonic rocks of Cox et al. (1979) by Wilson (1989). The data presented in Table 2 suggest some differences in major oxides, trace elements and rare earth elements (REEs) which can be seen when Harker's variation diagrams are constructed (Fig. 6). These diagrams indicate very distinct distinction between metagabbros and fresh gabbros where there is relative SiO_2 enrichment and depletion in the two varieties, respectively, which can be attributed to silica release upon breakdown of feldspars because of metamorphic and subsequent alterations (Mohamed and hassanen 1996). Variation in major elements and some trace elements is moderate to wide in case of the metagabbros due to mobility during metamorphism in which they become enriched in Mn, Ti, Fe, V and Ba. On the other hand, such variations in fresh gabbros are very limited or even negligible and they are generally enriched in Ca, Al, Ni and Sr. The spider multi-elemental diagram (Fig. 7a) shows relative enrichment of normalized trace elements to the primitive mantle in the southern intrusion of metagabbros at the Wadi Shuwas. The same observation is

Table 2 Chemical composition of the Ablah-Shuwas gabbroic rocks

Sample no.[a]	10 ($n = 3$)	9 ($n = 3$)	99 ($n = 3$)	11 ($n = 4$)	12 ($n = 3$)	6 ($n = 3$)	66 ($n = 4$)
Oxides (wt%)							
SiO_2	46.9	47.39	46.36	48.5	48.3	47.34	48.17
TiO_2	0.44	0.29	0.27	0.83	0.88	2.7	2.54
Al_2O_3	25.47	25.3	22.98	18.42	17.63	16.2	16.64
Fe_2O_3	3.11	4.56	5.83	6.93	7.46	12.14	11.83
CaO	10.73	11.73	11.14	9.39	9.71	7.33	7.69
MgO	3.67	5.42	8.64	7.75	8	5.41	4.36
Na_2O	2.63	2.89	2.45	3.12	2.94	3.85	4.25
K_2O	2.36	0.15	0.13	0.88	0.91	1.23	1.05
MnO	0.05	0.06	0.07	0.1	0.11	0.17	0.17
P_2O_5	0.06	0.05	0.04	0.08	0.07	0.56	0.66
L.O.I.	3.95	1.62	1.13	3.03	3.04	1.64	1.92
Total	99.46	99.54	99.06	99.15	99.22	98.63	99.38
Trace elements (ppm)							
Ba	231	230	128	432	444	454	497
Be	<1	<1	<1	<1	<1	1	4
Co	18.8	31.9	51.6	33	35	39.6	41.7
Cs	0.2	<0.1	<0.1	0.5	0.8	0.8	0.4
Ga	16.3	17.2	15	16.6	15.8	22.7	24.6
Hf	0.5	0.5	0.3	0.5	0.6	4.9	7.1
Nb	1.1	0.8	0.5	1.5	1.6	10.5	15.2
Rb	32.3	1.3	0.5	10.6	10.5	22.2	17.2
Sn	<1	7	<1	<1	<1	4	5
Sr	1858.5	1198.8	1207.6	1139.6	1093.5	798.7	931.7
Ta	<0.1	0.1	<0.1	0.1	0.2	0.5	0.7
Th	1.2	<0.2	<0.2	<0.2	<0.2	1.8	1.4
U	0.3	0.3	<0.1	0.4	0.1	1.2	0.7
V	37	34	31	101	121	232	238
W	31.6	33.4	25.5	17.3	21.4	8.2	22.3
Zr	20.6	18.7	11.4	21.4	23.8	253	310.5
Y	2.7	2.9	2.1	4.7	5.6	25.8	34.1
Mo	0.3	0.6	0.1	<0.1	0.3	0.8	0.7
Cu	3.4	59.6	167.6	80.3	92.5	45.2	48.8
Pb	1.6	8.4	2.5	0.7	0.7	17.9	13.7
Zn	16	18	30	27	23	54	59
Ni	69.1	94.7	236.9	85.9	90.5	42.8	25.9
As	0.7	2.4	0.7	9.4	9.1	1.4	1
Cd	<0.1	<0.1	<0.1	<0.1	<0.1	<0.1	<0.1
Sb	<0.1	<0.1	<0.1	<0.1	<0.1	<0.1	<0.1
Bi	<0.1	<0.1	<0.1	<0.1	<0.1	<0.1	<0.1
Ag	<0.1	<0.1	<0.1	<0.1	<0.1	<0.1	<0.1
Au	<0.5	1.5	3.9	1.1	1.4	1.2	<0.5
Hg	<0.01	<0.01	<0.01	<0.01	<0.01	<0.01	<0.01
Tl	<0.1	<0.1	<0.1	<0.1	<0.1	0.1	<0.1
Se	<0.5	<0.5	<0.5	<0.5	<0.5	<0.5	<0.5
REE (ppm)							
La	3.1	2.6	2	3.6	3.5	23.3	32.7
Ce	6.8	6.2	4.8	8.1	8.2	57.3	79.8
Pr	0.85	0.7	0.57	1.12	1.13	7.58	10.62
Nd	4.2	2.9	2.6	5.2	5.9	33.4	44.8

Table 2 continued

Sample no.[a]	10 ($n = 3$)	9 ($n = 3$)	99 ($n = 3$)	11 ($n = 4$)	12 ($n = 3$)	6 ($n = 3$)	66 ($n = 4$)
Sm	0.65	0.61	0.59	1.32	1.33	7.56	9.77
Eu	0.51	0.53	0.49	0.82	0.91	2.44	2.71
Gd	0.7	0.72	0.54	1.24	1.55	6.85	8.62
Tb	0.11	0.11	0.08	0.21	0.23	0.97	1.22
Dy	0.55	0.59	0.44	0.97	1.35	5.49	6.47
Ho	0.09	0.14	0.11	0.21	0.29	1	1.27
Er	0.29	0.41	0.24	0.51	0.73	2.78	3.5
Tm	0.04	0.05	0.04	0.06	0.09	0.37	0.48
Yb	0.29	0.21	0.18	0.41	0.47	2.41	2.99
Lu	0.04	0.05	0.03	0.07	0.09	0.32	0.45

Geographic coordinates are given in Table 1, and analyses in full are given in Appendix 1

[a] 10: Anorthositic olivine gabbro, 9 and 99: Olivine gabbro, 11 and 12: Northern metagabbros, 6 and 66: Southern metagabbros. Number of analyses is given as (*n*) between brackets

shown in Fig. 7b where the normalized REEs patterns of the southern intrusions show very clear enrichment in total REE compared with the northern metagabbros at the Wadi Raniyah. Another distinction between southern and northern metagabbros is the absence of any Eu anomaly in the former (Fig. 7b).

Mineral chemistry

The full chemical analyses of silicate and non-silicate minerals are determined by electron microprobe and are useful for determining petrogenetic indicators related to the evolution of gabbroic rocks in the Ablah-Shuwas area. The electron microprobe analyses are given in Appendices 2 and 3 for the metagabbros and fresh gabbros, respectively. Sample and spot numbers are specified for each mineral. These supplementary data can be accessed at: (*To be defined by the journal upon final editing*).

Feldspars

As expected for plagioclase in a metagabbro, it is sodic to intermediate. It ranges from andesine (An = 36.19) to albite (An content = 1.2–36.3). In the fresh gabbros, it is calcic plagioclase (Fig. 8a). Calcic plagioclase in fresh gabbro ranges from bytownite to labradorite with An content = 76–59.5. Only one analysis of plagioclase gives An content ~90 which is typical anorthite. In the metagabbros, albitization converts calcic plagioclase to oligoclase–albite.

Olivines and pyroxenes

The fresh gabbros at Wadi Raniyah preserve important primary magmatic minerals, namely olivine and pyroxene. They occur mostly as cumulus phases with a tendency of clinopyroxene toward intercumulus. The chemical analyses of olivine (Appendix 2) indicate forsterite composition with Mg# of 77.5–80.9. In highly fractionated fresh gabbros such as the anorthositic gabbro, fayalite end-member compositions increase and the Mg# = 56.7. Mg# is calculated as 100MgO/(MgO + FeO) in mole percent. The considerable fayalite component (up to 22.5) indicates a more evolved mafic magma. Cumulus clinopyroxene is diopside, and sub-solidus symplectitic orthopyroxene is clinoenstatite and minor pigeonite (Fig. 8b).

Amphiboles

Amphibole in the metagabbros is calcic (magnesio-hornblende at core and actinolite at rim) (Fig. 9c), with variable amounts of TiO_2 (up to 2.36 wt%). Ghoneim (1988) obtained similar amphibole composition in the arc-related metagabbros in Egypt that represent the northern extension of mafic arc magmatism in the middle and southern Arabian Shield in Saudi Arabia. Despite being metagabbros, the amphiboles preserve their igneous origin (Fig. 9d). This is consistent with the low-grade of metamorphism assigned to the adjacent volcano-sedimentary arc rocks of the Jeddah Group (Johnson et al. 2011). On the other hand, intercumulus Ti-rich or brown amphiboles in the fresh gabbros are calcic and range in composition from pargasite to actinolite–tremolite according to the classification of Leake et al. (1997).

Dark mica

Analyses of dark mica in the fresh gabbros indicate typical biotite composition of igneous origin (Rossi and Chévremont 1987) which is a Mg-rich variety (Fig. 10a). It is characteristic of primary mica in mafic rocks with little re-equilibration (Nachit et al. 1985). Fe biotite is common in evolved felsic rocks such as granite instead. A preliminary estimate of crystallization temperature of biotite ranges

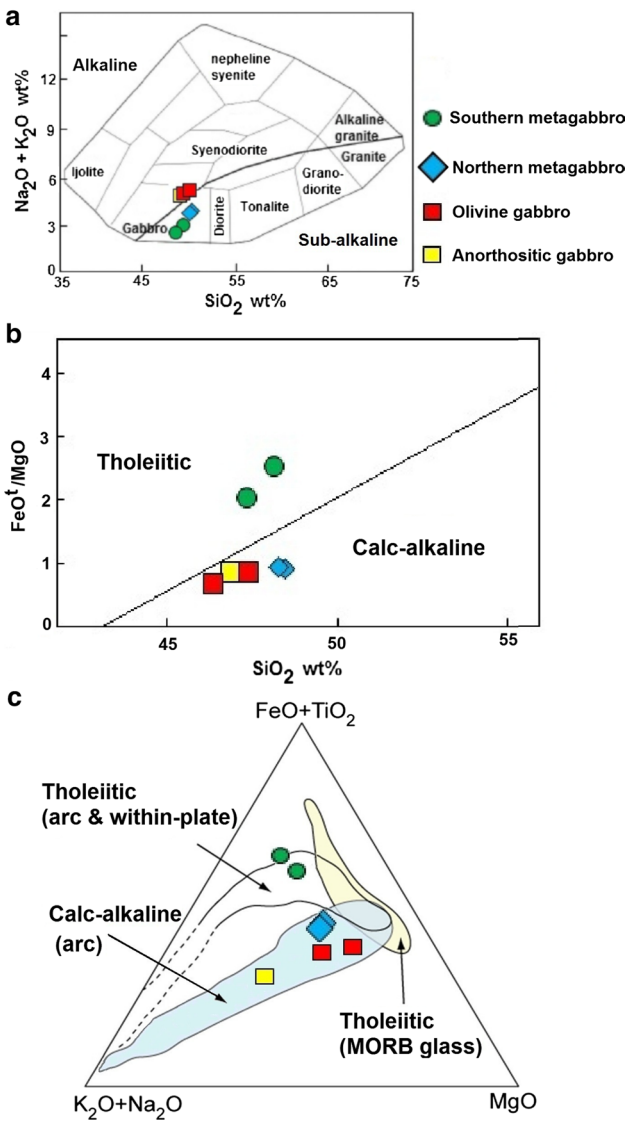

Fig. 5 **a** Classification of the gabbroic rocks using the diagram of Cox et al. (1979) modified by Wilson (1989). **b** Magma type diagram of Miyashiro (1975). **c** Plots of the gabbroic rocks on the AFM diagram with fields of magma type and tectonic setting following the trends defined by Irvine and Baragar (1971). Note the metagabbros represent both tholeiitic and calc-alkaline compositions

from 600 to 700 °C according to the semi-quantitative plots of Henry et al. (2005) (Fig. 9b).

Fe–Ti oxides

TiO_2 in magnetite from the metagabbros is 0–0.29 wt% only (Appendix 1). Ilmenite is highly altered to rutile, hematite and titanite. Ilmenite is Mn-rich (up to 6.41 wt% MnO), whereas Mg is minor (0–0.23 wt% MgO). Rutile is ferro-rutile and FeO content is 2.43–11.27 wt%. Titanite is also ferro-titanite and FeO is 0.86–2.94 wt% and one analysis gives 9.87 wt% FeO.

In the fresh gabbros at the Wadi Raniyah, magnetite is almost a Ti-free or normal variety. TiO_2 in magnetite is minimal (0.10–0.62 wt%) (Appendix 2). Ilmenite is altered to minor rutile and titanite because there is no metamorphism. Rutile is not a ferro-rutile and its FeO content amounts 0.19–0.59 wt%. Titanite is also Fe-poor and FeO is 0.62 wt%.

Discussion

Mafic arc magmatism and source material in the Arabian Shield

Whole-rock geochemistry is very helpful to decipher the nature of magma from which rocks crystallize. The multi-elemental diagram normalized to primitive mantle for both metagabbros and fresh gabbros (Fig. 7a) display similarity in anomalies like the distinct Sr and Ti anomalies but with relative enrichment of the normalized elements in the metagabbros especially those of the southern intrusion. It seems that the positive Sr anomaly exists regardless of the sericitization of Ca plagioclase in the metagabbros. This can be also another clue for negligible or very low-grade regional metamorphism in the Ablah-Shuwas area. Further south in the Arabian Shield, regional metamorphism might reach up to lower amphibolite facies (Farier 1985).

The northern and southern metagabbros show a slight LREE enrichment over the HREE. It is evident that there is an increase in ΣREE with differentiation. The southern metagabbros are enriched in LILE (e.g., Ba, Rb and Sr) and depleted in HFSE (e.g., Ta, Nb, Hf, Zr and Y) (Fig. 7b). Figure 7, together with Fig. 8a, strongly indicates shoshonitic and high-K calc-alkaline magmatism related to a lithospheric mantle source with earlier modification by subduction (Saunders et al. 1980). On the other hand, the younger fresh gabbros, particularly the anorthositic varieties, show enrichment of LREE and depletion of HREE which is consistent with the pronounced Eu anomaly (Fig. 7b) and fractional crystallization (Helmy and El-Mahallawi 2003). Trace elements and REE compositions of Wadi Raniyah fresh gabbros indicate derivation from an enriched mantle source (e.g., garnet lherzolite) by little to moderate partial melting (~5–10 %), which can reach up to 15–30 % in the northern parts of the shield (Abu Anbar 2009). The geochemical data presented here are interpreted to conclude that the metagabbros are arc-related (late Cryogenian), either tholeiitic (southern intrusion) or calc-alkaline (northern intrusion). Most likely the fresh gabbros reflect the late- to post-collisional phase. Therefore, metagabbros in the Arabian–Nubian Shield pre-date extension associated with orogenic collapse (Johnson 2006; Johnson et al. 2001, 2011, 2013; Abdel Halim et al. 2016).

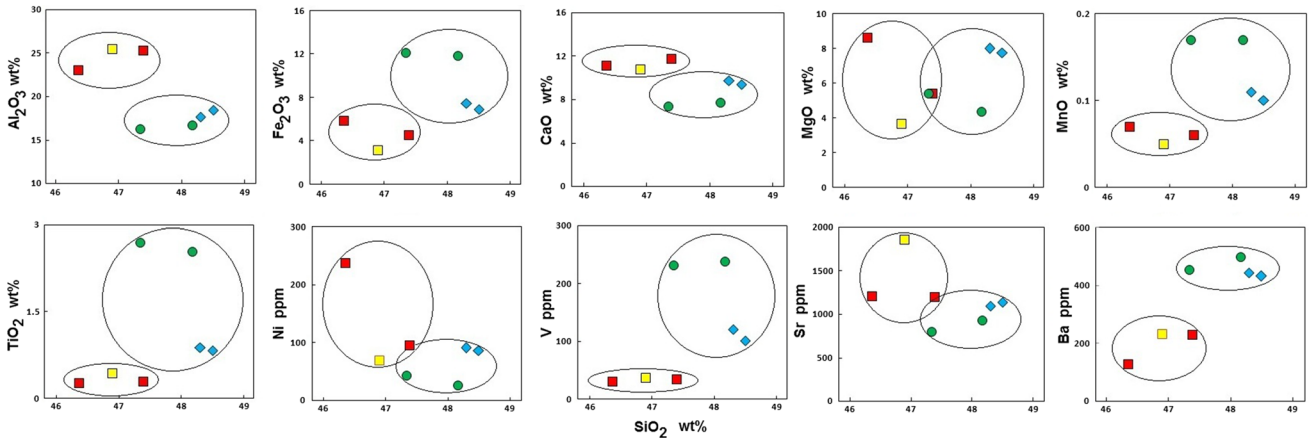

Fig. 6 Harker's variation diagrams of SiO_2 versus some major oxides and trace elements, with distinct separation of the metagabbros from the fresh gabbros. *Symbols* are as shown in Fig. 5

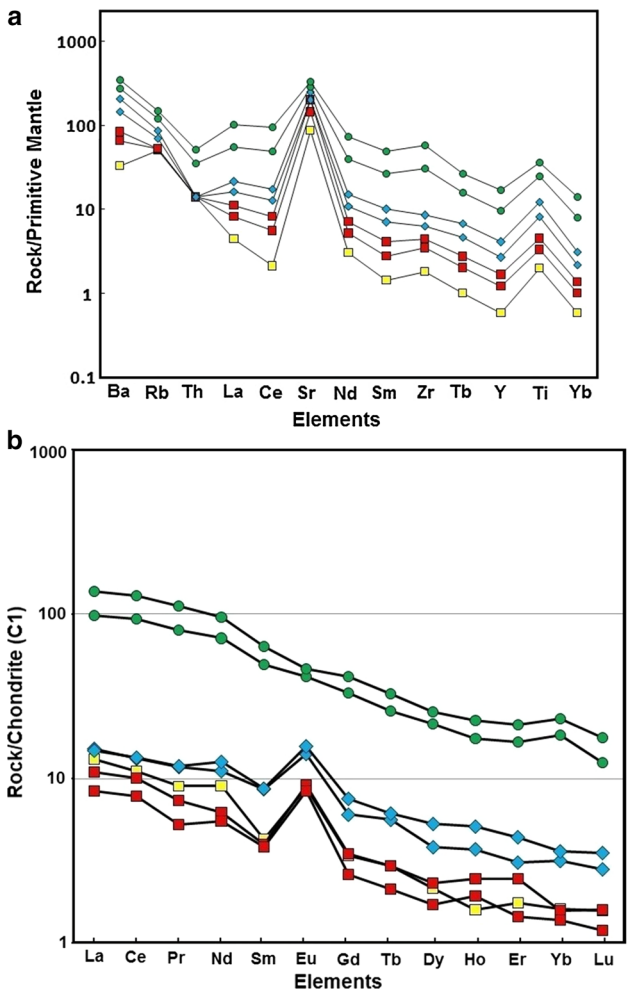

Fig. 7 **a** Contents of some incompatible and large-ion lithosphere elements in the gabbroic rocks normalized to the primitive mantle. **b** REE normalized patterns of the metagabbros. Normalization values of both primitive mantle and chondrite are taken from Sun and McDonough (1989). *Symbols* are as shown in Fig. 5. Note the similarity between the older and younger gabbros

The La/Yb and Nb/La ratios in the Raniyah fresh gabbros (15.55–18 and 0.17–0.24, respectively) are characteristic of post-collisional magmas (Khalil et al. 2015). A possible origin for this magma was during the post-collisional stage of an earlier continental arc with Zr/Y ratios in the range of 5.43–7.63 (Khalil et al. 2015). The N–S trending Ablah basin itself formed post-amalgamation and was contemporaneous with or post-emplacement of A-type granitoids (Genna et al. 1999; Johnson et al. 2001). The Ablah basin started to form after the waning of Pan-African orogenesis and emplacement of mafic arc intrusions and A-type granites by crustal thinning, extension, subsidence and development of transpressional regime that reflects progressive convergence between east and West Gondwana (Stern 1994; Genna et al. 2002; Johnson 2003; Stern and Johnson 2010; Hamimi et al. 2013).

The northern metagabbro of the Ablah-Shuwas area is derived from a tholeiitic mafic magma, whereas the southern metagabbros are calc-alkaline (Fig. 5b). Nevertheless, both intrusions characterize an arc setting (Fig. 5c) and hence are comparable to the metagabbro diorite complexes in the Nubian Shield that formed ~880 Ma ago by subduction-related calc-alkaline magmatism in island-arcs where the magma originated from partially melted amphibolites or hydrous mafic magma (e.g., Helmy et al. 2008; Qaoud and Abdelnasser 2012). The Wadi Raniyah fresh olivine, olivine–hornblende and anorthositic gabbros with very characteristic biotite are cumulate products of differentiated mafic arc magma with prominent interstitial hydrous minerals that increase with fractional crystallization (Claeson and Meurer 2004; Helmy et al. 2008). In this respect, fresh or younger gabbros in the Arabian–Nubian Shield are post-collisional and did not form in a proper within-plate setting like that suggested by Mohamed and Hassanen (1996), Basta (2015) and Abd El-Rahman (2015). Similarly, some

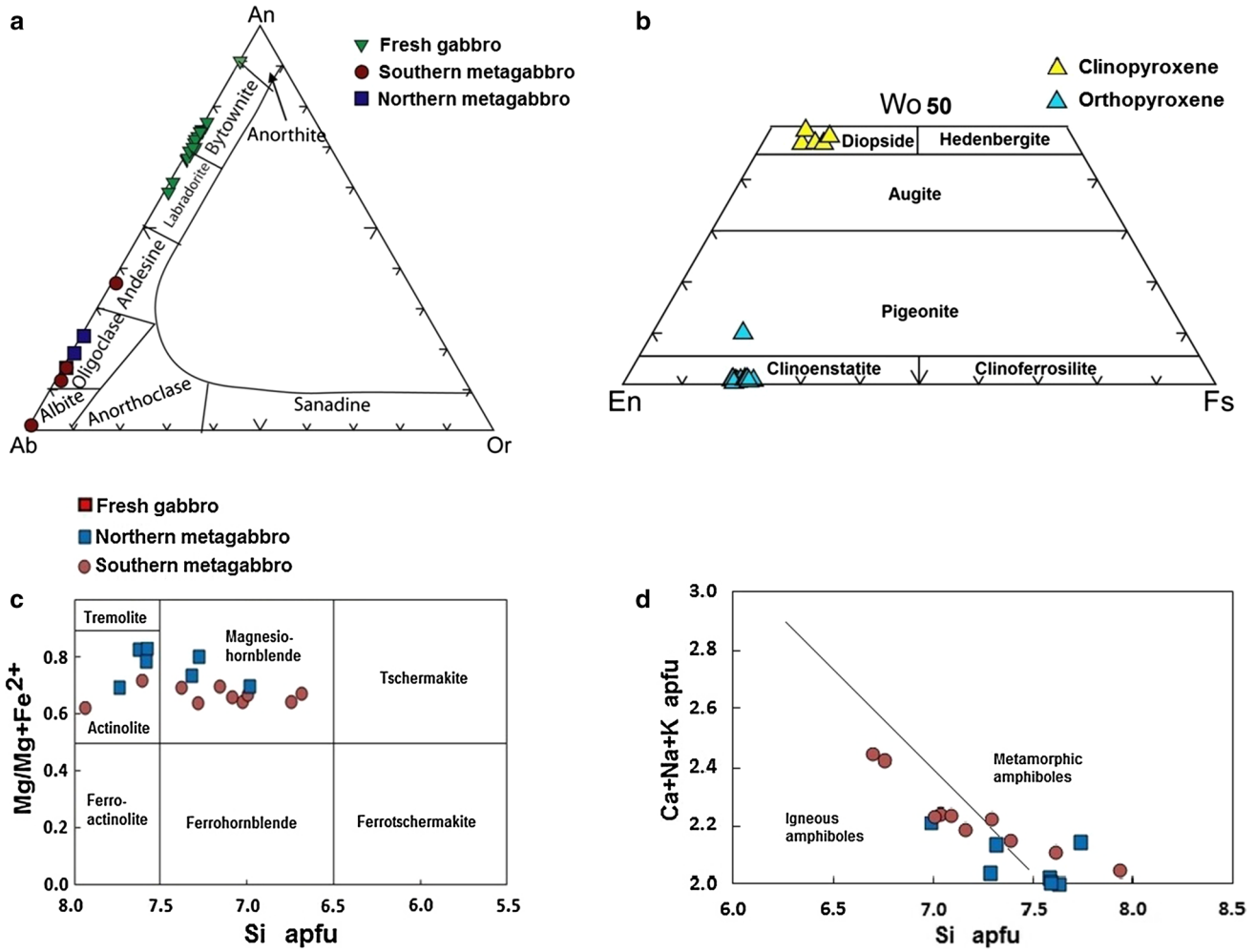

Fig. 8 **a** Plots of plagioclase composition in the gabbroic rocks (Deer et al. 1992). **b** Quadrilateral classification of pyroxene in the fresh gabbros (Morimoto et al. 1988). **c** Composition of amphiboles in the metagabbros (Leake et al. 1997). **d** Distinction between igneous and metamorphic amphiboles in the metagabbros (Giret et al. 1980). *Apfu* atoms per formula unit

workers (e.g., Azer and El Gharabawi 2011; Abdel Karim 2013) believe that the younger gabbros in the northern Arabian–Nubian Shield continued to form as post-collisional intrusions at the time that they ceased being emplaced in the middle and southern parts of the shield in Saudi Arabia. In the northern part of the Arabian–Nubian Shield, delamination of lithospheric mantle allowed asthenosphere to rise rapidly, allowing production of mafic melt by partial melting that infiltrated the base of the crust to produce post-collisional younger gabbros (Khalil et al. 2015).

Crystallization temperature for the fresh Raniyah gabbros

We use the new Al-in-olivine geothermometer of Coogan et al. (2014) (spine inclusions are absent from olivine crystals). It is based on Al and Ni cations in structure and variation in the Fo content. Fo = 77.5–81. The resulting temperature ranges from 1037 to 1085 °C (Table 3). The lower temperature of 765 °C represents a destabilized olivine rim in symplectite where Fo = 57 (Table 3).

Clino- and orthopyroxene are not formed simultaneously in the fresh gabbros; consequently, they are not controlled by the same equilibrium conditions, and hence, the equations to estimate temperature using the two pyroxene pairs are not applicable. The temperature of clinopyroxene ranges from 628 to 875 °C according to geothermometer of Nimis and Taylor (2000). At 875 °C, pressure is high = 5.2 kbar which indicates deeper level of the intrusion (Table 3). At 628 °C, pressure is lower (1.6 kbar) consistent with a shallower level of intrusion (where pressure is calculated according to Putirka 2008). Brown amphibole is a Ti-rich igneous variety where TiO_2 amounts up to 3.21 wt%. The temperature of brown amphibole is calculated by the method of Helz (1973) which depends on the Ti content. The temperature ranges from 794 to 558 °C (Table 3). This

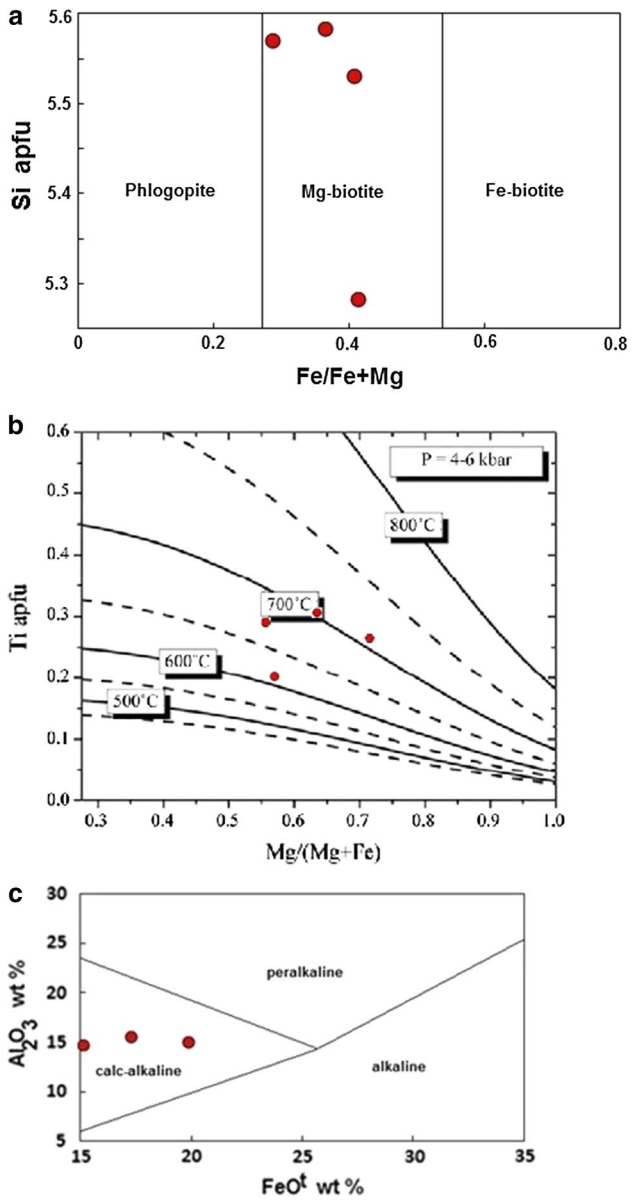

Fig. 9 **a** Nomenclature of dark mica in the fresh gabbros as Mg-rich biotite (Deer et al. 1966). **b** Tentative crystallization temperature of biotite (Henry et al. 2005). **c** Calc-alkaline nature of magma (Abdel Rahman 1994)

suggests that brown amphibole starts to crystallize just after and during formation of cpx. Similar temperature ranges are described for arc-related fresh gabbros in the northern tip of the Arabian–Nubian Shield, for example 961–674 °C (average of 817 °C) and for the Nesryin younger gabbros in Sinai that were emplaced at 617 ± 19 Ma (Abu Anbar 2009). More recently, Khalil et al. (2015) reported a similar range of crystallization temperatures (970–750 °C) for the fresh younger gabbros at El-Mahash area in the northern Arabian–Nubian Shield, particularly in the Sinai Peninsula of Egypt. Biotite can be divided into magmatic (M), re-equilibrated (R) and hydrothermal (H) types according to petrographic and compositional criteria. Magmatic biotite crystallizes directly from a silicate melt, re-equilibrated biotite forms during cooling history of magma, and hydrothermal types result from potassic and sericitic hydrothermal alteration (Nachit et al. 2005; Parsapoor et al. 2014). The Mg-rich biotite variety in the Raniyah fresh gabbros is characteristic of primary mica in mafic rocks with little re-equilibration. Crystallization temperatures for biotite range from 600 to 700 °C (method of Henry et al. 2005) (Fig. 9b). The concentration of Ti in biotite is very sensitive to temperature and oxygen fugacity, making it possible to use biotite to obtain reliable temperature estimates in igneous and metamorphic rocks (Patino Douce 1993). However, because the thermometry of Henry et al. (2005) is calibrated for biotite from pelitic rocks rather than igneous systems (Fig. 9a), we do not recommend its application to the Raniyah fresh gabbros.

Estimation of pressure (magmatic vs. metamorphic)

The amphibole shows signature of both igneous and metamorphic nature (Fig. 8d). This indicates a slight redistribution of cations in the amphibole structure due to low-grade greenschist facies metamorphism. Quantitatively, metamorphic amphibole in the studied metagabbros crystallizes at a 1.05–3.25 kbar, whereas it lies in the range of 1.6–5.4 kbar in the case of fresh gabbros.

For both cases, pressure is calculated by the barometers of Helz (1973) and Putirka (2008), respectively (Table 3). Low pressures associated with arc-related metagabbros in the Nubian Shield have previously been obtained from amphibole chemistry (Ghoneim 1988). Pressure estimates in the ranges of 2.8–5.6, 4.01–6.16 and 5.4–6.6 kbar were also obtained for some arc-related and post-collisional younger gabbros in Sinai and the Eastern Desert of Egypt as a part of the northern Arabian–Nubian Shield (Abu Anbar 2009; Ali-Bik et al. 2014; Khalil et al. 2015, respectively). This is broadly consistent with our results and equivalent to c. 12–15 km depth of emplaced intrusions.

Oxygen fugacity during metamorphism

Oxygen fugacity is qualitatively estimated from the composition of calcic amphibole. As shown in Fig. 10d, the amphiboles from Wadi Shuwas metagabbros form at high fugacity indicating oxidizing conditions. The amphibole formed at low pressure (~1–3 kbar) and in oxidizing condition due to high f_{O_2} (Fig. 10d). As a consequence of the edenite substitution, coupled with a Ti–Tschermak substitution, there is temperature-sensitive rimward increase in total Al, Ti, Na and K (Bachmann and Dungan 2002). This explains the differences in temperatures of cores and rims

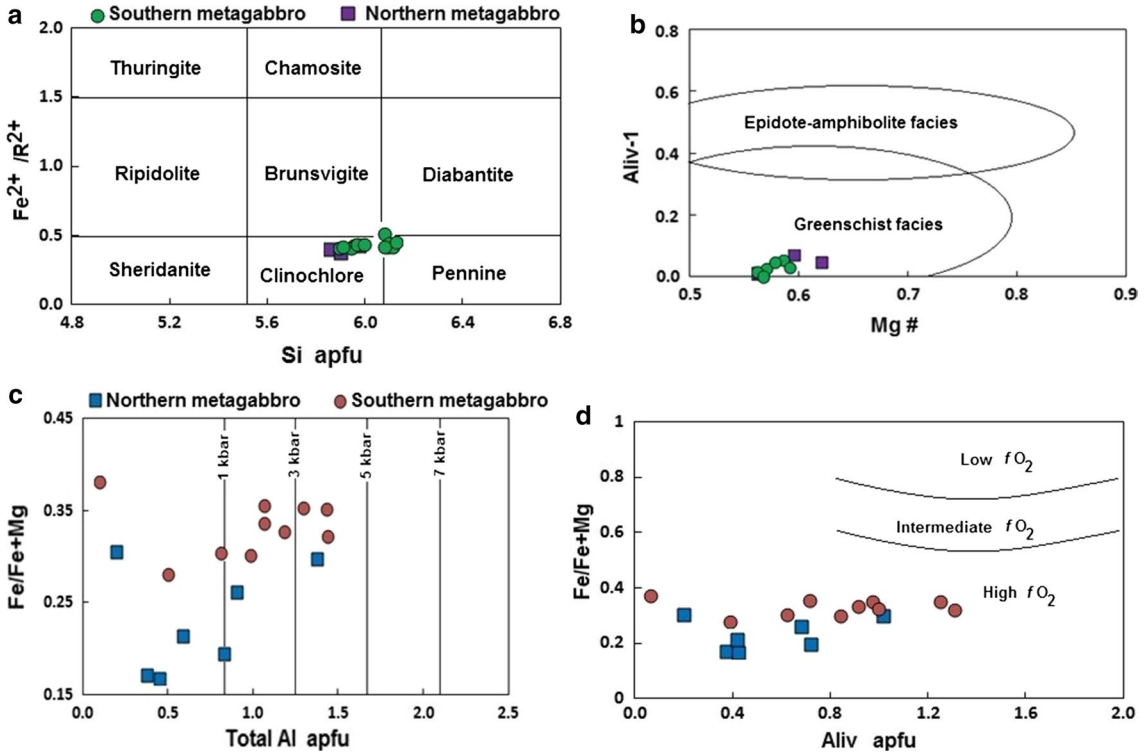

Fig. 10 **a** Composition of chlorite (mainly clinochlore) in the metagabbros (Foster 1962). **b** Greenschist facies conditions of regional metamorphism (Bailey 1988). **c** Up to 5 kbar pressure conditions for calcic amphibole in metagabbros (Anderson and Smith 1995). **d** High oxygen fugacity during amphibole crystallization (Anderson and Smith 1995)

Table 3 Temperature–pressure estimates for the Ablah gabbroic rocks

Rock type	*T* (°C)	*P* (kbar)	Calculation method	Mineral used
Metagabbro	445–727	–	Holland and Blundy (1994)	Plagioclase–amphibole pairs
	–	1.05–3.25	Helz (1973)	Amphibole
	247–275[a]	–	Kranidiotis and MacLean (1987)	Chlorite
Fresh gabbro	1037–1086	–	Coogan et al. (2014)	Olivine
	628–875	–	Nimis and Taylor (2000)	Clinopyroxene
	–	1.6–5.4	Putirka (2008)	Clinopyroxene
	558–794	–	Helz (1973)	Amphibole
	765[b]	–	Coogan et al. (2014)	Olivine

[a] Temperature of retrogressive metamorphism

[b] Destabilization temperature of olivine in symplectite

in the amphiboles from the Wadi Shuwas metagabbro. Formation of actinolite at the outer peripheries of hornblende and its temperature-induced Al-zoning is an indication of rejuvenation and remobilization of a preexisting near-solidus crystal mush in shallow intrusions of mafic magma (Bachmann et al. 2002).

Temperature of chlorite alteration and magma type

Biotite in the fresh gabbros of Wadi Raniyah is magmatic and its composition indicates a calc-alkaline magma (Fig. 9c, d). Chemistry of chlorite in the metagabbros can be also helpful to calculate temperature of regional metamorphism and metamorphic grade, since the majority of chlorite species are sensitive to temperature and hence the types of common substitutions and occupancies of Fe, Mg and Al in both tetrahedral and octahedral sites (Foster 1962; Cathelineau 1988; Laird 1988; Inoue et al. 2009, 2010). Analyses of chlorites from metagabbros at Wadi Shuwas indicate they represent clinochlore to pennine (Fig. 10a). Structurally, these chlorites are tri/dioctahedral (Bailey 1988) and also considered to be Mg chlorites (occasionally

Fe chlorite) or Type I of Zane and Weiss (1998) who also consider Al-rich end members as Type II chlorites. Such a composition suggests simple ionic (Fe^{2+} for Mg) and Tschermak substitutions. Crystallization temperature of chlorites from low-grade metamorphic rocks and hydrothermal alteration zones can be calculated on the basis of Al cations and Fe/Fe + Mg ratio (Cathelineau and Nieva 1985; Jowett 1991). Minerals of the chlorite group show wide chemical variations depending on amount of divalent cations and their distribution among structural sites of each mineral (Foster 1962; Velde 1985; Wiewiora and Weiss 1990; Abdel Rahman 1995; Zane and Weiss 1998). The ratio of Fe/Fe + Mg (0.11–0.2) of low-grade metamorphic and hydrothermal chlorite is temperature independent in the range of 200–300 °C (Cho et al. 1988; Yau et al. 1988). Homogeneity of chlorite composition is a function of both the temperature of equilibration and its duration (Velde et al. 1991). On the other hand, diagenesis has little effect on chlorite Fe^{2+} and Mg distribution in chlorite that forms at 40–70 °C (Velde and Medhioub 1988; Velde et al. 1991).

Qualitative estimation of chlorite indicates it is formed in low-grade greenschist facies condition (Fig. 10b). Quantitative calculation of chlorite temperature using the equations of Kranidiotis and MacLean (1987) gives 247–272 °C for the northern metagabbro and 263–275 °C for the southern metagabbro (Table 3). These equations are calibrated for chlorite with 0.18–0.64 Fe/Fe + Mg and are appropriate for our samples. The temperatures obtained suggest formation of chlorite and Ca epidote at the expense of igneous calcic amphibole as retrograde phases typical of greenschist facies conditions (Bailey 1988) (Fig. 10b). The temperature of retrograde metamorphism was determined by the method of Kranidiotis and MacLean (Table 3). The calibrations associated with other chlorite thermometers (e.g., Bourdelle et al. 2013; Vidal et al. 2005, 2006; Inoue et al. 2010) are outside the compositional range of Ablah metagabbro and therefore not applicable. The analyzed chlorite is indicative of calc-alkaline magma (Abdel Rahman 1994).

Fe–Ti oxides and their role in petrogenesis

Due to high-temperature deuteric alteration followed by low-grade metamorphism, ilmenite is highly altered to rutile, hematite and titanite. It is Mn-rich (up to 6.41 wt% MnO) and Mg-poor (0–0.23 wt% MgO). It seems that Mn content in ilmenite is controlled by exsolution–oxidation, f_{O_2} and the rate of magmatic differentiation. For example, exsolved ilmenite lamellae have up to 1.48 wt% in some titanium–phosphorus ores hosted by gabbros which is much higher than in homogeneous ilmenite (Mehdilo and Irannajad 2010). Mn in ilmenite increases with differentiation. Gabbros usually have ilmenite with low Mn and Mg contents (Haggerty 1976). $MnTiO_3$ (pyrophanite) increases from ~20 Mol% in gabbros to ~30 Mol% in more differentiated compositions (Tarassova et al. 2009). Ilmenite from the metagabbro of Wadi Shuwas has high Mn content consistent with low-T alteration at high f_{O_2} (Buddington and Lindsley 1964; Anderson 1968; Sasaki et al. 2003; René 2011). It seems that enrichment in ilmenite is enhanced by volatiles that are enriched during high phosphorous activity (Sasaki et al. 2003; Mehdilo and Irannajad 2010). Alteration of ilmenite to rutile and titanite also enhances enrichment of Mn in ilmenite (Dorfler et al. 2014). Ilmenite composition indicates magma derivation from shallow rather than deep mantle (Haggerty and Tompkins 1984; Haggerty et al. 1985; Golubkova et al. 2014).

Origin of symplectite in the Raniyah fresh gabbros

Symplectites are sub-solidus intergrowths that form in many igneous and metamorphic rocks (Vernon 2004) and in most cases their formation is related to variations in pressure (Griffin 1971; Carswell et al. 1989; Morishita et al. 2001; Turner and Stüwe 1992). Symplectite mineralogy is represented by a variety of silicates minerals together or silicates intergrown with oxide phases such as magnetite, ilmenite and spinel (Cruciani et al. 2008). Symplectitic intergrowth of orthopyroxene–magnetite represent an eutectic-like texture that results from simultaneous coprecipitation of the two minerals in a crystal mush, less than 20 vol% residual melt, when Mg-rich olivine reacts with late-stage magmatic liquids (Ambler and Ashley 1980). With respect to orthopyroxene–magnetite symplectite, as in the Wadi Raniyah fresh gabbros, it is argued to form by sub-solidus reaction, but other processes such as exsolution and diffusion can also be involved (Barton and Van Gaans 1988). As mentioned previously, the younger fresh gabbros provide evidence of cumulus olivine destabilization at ~765 °C. This temperature is almost the same as those obtained for similar symplectites elsewhere in the world (e.g., 740–790 °C; Cruciani et al. 2008). We agree with these authors that an increase in water activity (aH_2O = 0.5–1) enhances the formation of symplectitic intergrowths in gabbros that initially form at relatively high depth and pressure (~5.2 kbar) prior to their emplacement at shallower levels. Consequently, we suggest that symplectite formation in Wadi Raniyah gabbros involved pervasive sub-solidus oxidation which resulted in the breakdown of olivine to clinoenstatite and Ti-free magnetite. In this respect, we disagree with Efimov and Malitch (2012) that symplectites form in the solid state because the Wadi Raniyah gabbros continue to crystallize hydrous phases (amphibole and biotite) due to penetrating fluids in the rock. The source and timing of hydration is most probably late-magmatic and/or deuteric (Claeson 1998), but not hydrothermal (Turner and Stüwe 1992) as indicated by

textures, mineral paragenesis and sequence of crystallization. However, symplectites in the fresh gabbros from Wadi Raniyah show no evidence of formation by solid solution, cooperative nucleation or diffusion which is in agreement with Barton and Van Gaans (1988). Free oxygen is needed to oxidize olivine and this results from dissociation of penetrating water when gabbros are still hot at the initial stage of emplacement (Efimov and Malitch 2012). The present textural, mineralogical and P/T estimates suggest that morphological variation in Ti-poor magnetite in symplectitic orthopyroxene (drop-like to massive, vermicular and linear) might result from one and/or all of the following: rate of oxidation, variation in water activity (aH_2O), localization to certain crystallographic planes and variability of pressure. The drop-like to massive symplectite might represent the prototype that grades to vermicular and linear types as the process of replacement proceeds. Ambler and Ashley (1980) called the prototype an "embryonic" symplectite that can evolve until complete pseudomorphic replacement gives rise to other types.

Conclusions

The metagabbros in the Ablah-Shuwas area are tholeiitic to calc-alkaline and formed during arc genesis. This characterizes proper arc- and collisional-related late Cryogenian intrusions emplaced at ~850–780 Ma. On the other hand, the younger fresh gabbros are exclusively calc-alkaline and might represent syn- to post-collisional intrusions prior to the emplacement of A-type granitoids of distinct post-collisional setting. Although supported by field relationships that clearly demonstrate that the majority of the our gabbroic samples are intruded by post-collisional A-type monzogranite, syenogranite and syenite, from a geochronological point of view absolute age data are lacking. Following the IUGS time scale (Cohen et al. 2013), the fresh younger gabbros are presumed to be ≥630 Ma (i.e., Ediacaran) which is the age of post-collisional monzogranite that intrudes them (Moufti 2001). The calc-alkaline magmatism that produced the metagabbros is related to a lithospheric mantle source previously modified by subduction (Abu Anbar 2009). The fresh gabbros may have been produced by partial melting of enriched mantle source (e.g., garnet lherzolite). The A-type granitoids themselves have either a mantle origin or a Rb-depleted crustal source owing to low (0.7035–0.7038) $^{87}Sr/^{86}Sr$ initial ratios (Moufti 2001). The final emplacement of A-type granitoids coincided with the early phase of post-collisional sedimentation or formation of the molasse-type sediments (Genna et al. 1999).

The metagabbros at Wadi Shuwas were slightly metamorphosed under low-grade greenschist facies conditions. Their calcic amphiboles are typical of calc-alkaline complexes. The amphibole formed at low pressure (~1–3 kbar) under oxidizing conditions with high f_{O_2}. The temperature for amphibole crystallization reached up to 727 °C. Crystallization of chlorite occurred at 247–275 °C and indicates a retrograde greenschist facies path. Both rutile and titanite are Fe-rich indicating high Fe activity during alteration of ilmenite. Ilmenite is Mn- and Fe-rich, consistent with high f_{O_2} and the hemoilmenite mineral composition (Spencer and Lindsley 1981; Sasaki et al. 2003; Tarassova et al. 2009).

The trajectory of magmatic crystallization in the fresh Raniyah gabbros can be summarized as follows: Formation of olivine and plagioclase as cumulus phases at high temperature ~1050 °C, followed by formation of intercumulus clinopyroxene (up to 875 °C) possibly contemporaneous with destabilization of cumulus olivine and formation of symplectite and corona textures at ~765 °C. Intercumulus brown amphibole is formed between ~550 and 770 °C. Pressure is variable (5.4–1.6 kbar) possibly indicating polybaric levels of emplacement. Mg biotite is igneous and not formed during metamorphism, metasomatism or hydrothermal alteration. Chemistry of biotite is consistent with calc-alkaline magmatism. The presence of hydrous minerals and Mg and Ti contents suggest melt derivation from a metasomatized source. Detailed isotopic investigations are needed to distinguish between lower crust or mantle sources. Finally, fresh gabbros at Wadi Raniyah are calc-alkaline and represent Ediacaran post-collisional rather than within-plate intrusions. This is contrary to the conclusion reached by Mohamed and Hassanen (1996). The fresh Raniyah gabbros represent a well-defined post-collisional magmatic stage (620–590 Ma) in the Arabian–Nubian Shield that commenced with the emplacement of high-K calc-alkaline intrusions and concluded with A-type granitoids (Jarrar et al. 2003; Eyal et al. 2010; Morag et al. 2011; Khalil et al. 2015). However, we cannot exclude the possibility that some fresh gabbros are exclusively alkaline and formed in a within-plate setting as late as the Mesozoic like the alkaline gabbros and olivine monzogabbro (essexite) of Al-Kahfa area in the Eastern Desert of Egypt that intrude 585 ± 13 Ma molasse-type post-collisional sediments of the Hammamat Group (Akaad and Noweir 1980; Wilde and Youssef 2002).

Acknowledgments The authors are greatly indebted to the staff and assistants at the Department of Mineral Resources and Rocks at the King Abdulaziz University (Jeddah, Saudi Arabia) for the field facilities. Sincere help of Dr. Kamal Ali and Dr. Rami Bakhsh are greatly acknowledged especially with some logistics and whole-rock chemical analyses. Mr. Abdelmonem Habtoor made a great effort in grinding the samples and additional office work. The authors are grateful to Prof. Wolf-Christian Dullo (Editor-in-chief) and Prof. Victoria Pease for the kind handling of the manuscript and revision of English. The constructive comments and suggestions by Dr. Peter Johnson and an anonymous reviewer greatly helped to improve the manuscript.

References

Abd El-Rahman Y (2015) The Arabian–Nubain Shield from a mid-Cryogenian continental arc to Ediacaran post-collisional appinite-high Ba–Sr monzogranite suite: evidence from the South Um Mongul Area, NED, Egypt. Goldschmidt Conference 2015 Abstract. http://goldschmidt.info/2015/uploads/abstracts/finalPDFs/3.pdf

Abd El-Rahman Y, Helmy HM, Shibata T, Yoshikawa M, Arai S, Tamura A (2012) Mineral chemistry of the Neoproterozoic Alaskan-type Akarem Intrusion with special emphasis on amphibole: implications for the pluton origin and evolution of subduction-related magma. Lithos 155:410–425

Abdel Halim A, Helmy HM, Abdel Rahman Y, Yoshikawa M, Shibata T, Arai S (2016) Petrology of the Motaghairat mafic-ultramafic complex, Eastern Desert, Egypt: a high-Mg post-collisional extension-related layered intrusion. J Asian Earth Sci 116:164–180

Abdel Karim AM (2013) Petrology, geochemistry and petrogenetic aspects of younger gabbros from south Sinai: a transition from arc to active continental margin. Chem Erde 73:89–104

Abdel Rahman AM (1994) Nature of biotites from alkaline, calc-alkaline, and peraluminous magmas. J Petrol 35:525–541

Abdel Rahman AM (1995) Chlorites in a spectrum of igneous rocks: mineral chemistry and paragenesis. Mineral Mag 59:129–141

Abdelsalam MG, Stern RJ (1996) Sutures and shear zones in the Arabian–Nubian Shield. J Afr Earth Sci 23:289–310

Abu Anbar MM (2009) Petrogenesis of the Nesryin gabbroic intrusion in SW Sinai, Egypt: new contributions from mineralogy, geochemistry, Nd and Sr isotopes. Mineral Petrol 95:87–103

Akaad MK, Noweir AM (1980) Geology and lithostratigraphy of the Arabian Desert orogenic belt of Egypt between latitudes 25°35′ and 26°30′N. Inst Appl Geol Bull 3:127–136

Ali-Bik MW, Abdel Rahim S, Abdel Wahab W (2014) Hornblende gabbros of Wadi Az Zarib area, central Eastern Desert, Egypt: opaque mineralogy, geochemistry, tectonic setting and petrogenesis. Arab J Geosci 7:4009–4027

Ambler EP, Ashley PM (1980) Mineralogy and petrology of the Dutchmans.tfn gabbroic intrusion, South Carolina: discussion. Am Mineral 65:1302–1303

Anderson AT (1968) Oxidation of the La Blache Lake titaniferous magnetite deposits, Quebec. J Petrol 76:525–547

Anderson JL, Smith DR (1995) The effects of temperature and f_{O_2} on the Al-in-barometer. Am Mineral 80:549–559

Azer MK, El Gharabawi RI (2011) The Neoproterozoic layered mafic-ultramafic intrusion of Gabal Imleih, south Sinai, Egypt: implications of post-collisional magmatism in the north Arabian–Nubian Shield. J Afr Earth Sci 60:253–272

Bachmann O, Dungan MA (2002) Temperature-induced Al-zoning in hornblendes of the Fish Canyon magma, Colorado. Am Mineral 87:1062–1076

Bachmann O, Dungan MA, Lipman PW (2002) The Fish Canyon magma body, San Juan volcanic field, Colorado: rejuvenation and eruption of an upper crustal batholiths. J Petrol 43:1469–1503

Bailey SW (1988) Polytypism of 1:1 layer silicates. In: Bailey SW (ed) Hydrous phyllosilicates (exclusive of micas). Reviews in Mineralogy, vol 19. Mineralogical Society of America, pp 9–26

Bamousa A (2013) Infracambrian superimposed tectonics in the late Proterozoic units of Mount Ablah area, southern Asir Terrane, Arabian Shield, Saudi Arabia. Arab J Geosci 6:2035–2044

Barton M, Van Gaans C (1988) Formation of orthopyroxene-Fe–Ti-oxide symplectites in Precambrian intrusives, Rogaland, southwestern Norway. Am Mineral 73:1046–1059

Basta MS (2015) Petrology and geochemical characteristic of the younger gabbros of Wadi Shianite Area, Southeastern Desert, Egypt. Open J Geol 5:557–588

Be'eri-Shlevin Y, Katzir Y, Whitehouse M (2009) Post-collisional tectonomagmatic evolution in the northern Arabian–Nubian Shield: time constraints from ion-probe U–Pb dating of zircon. J Geol Soc Lond 166:71–85

Blasband BB (2006) Neoproterozoic tectonics of the Arabian–Nubian Shield. Dissertation, Utrecht University

Bourdelle F, Parra T, Chopin C (2013) A new chlorite geothermometer for diagenetic to low-grade metamorphic conditions. Contrib Mineral Petrol 165:723–735

Buddington AF, Lindsley DH (1964) Iron–titanium oxide minerals and synthetic equivalents. J Petrol 5:310–357

Carswell DA, Möller C, O'Brien PJ (1989) Origin of sapphirine-plagioclase symplectites in metabasites from Mitterbachgraben, Dunkelsteinerwald granulite complex, Lower Austria. Eur J Mineral 1:455–466

Cathelineau M (1988) Cation site occupancy in chlorites and illites as a function of temperature. Clay Miner 23:471–485

Cathelineau M, Nieva D (1985) A chlorite solid solution geothermometer: the Los Azufres (Mexico) geothermal system. Contrib Mineral Petrol 91:235–244

Cho M, Liou LG, Bird DK (1988) Prograde phase relations in the State 2-14 well metasandstones, Salton Sea geothermal field, California. J Geophys Res 93:13081–13103

Claeson DT (1998) Coronas, reaction rims, symplectites and emplacement depth of the Rymmen gabbro, Transscandinavian Igneous Belt, southern Sweden. Mineral Mag 62:743–757

Claeson DT, Meurer WP (2004) Fractional crystallization of hydrous basaltic 'arc-type' magmas and the formation of amphibole-bearing gabbroic cumulates. Contrib Mineral Petrol 147:288–304

Coogan LA, Saunders AD, Wilson RN (2014) Aluminum-in-olivine thermometry of primitive basalts: evidence of an anomalously hot mantle source for large igneous provinces. Chem Geol 368:1–10

Cohen KM, Finney S, Gibbard PL (2013) International chronographic chart: International commission on stratigraphy, Chronostrat Chart 2013-1. http://www.stratigraphy.org/index.php/ics-chart-timescale

Cox KG, Bell JD, Pankhurst RJ (1979) The interpretation of igneous rocks. Chapman & Hall, London

Cox GM, Lewis CJ, Collins AS, Halverson GP, Jourdan F, Foden J, Nettle D, Kattan F (2012) Ediacaran terrane accretion within the Arabian–Nubian Shield. Gondwana Res 21:341–352

Cruciani G, Franceschelli M, Groppo C, Brogioni N, Vaselli O (2008) Formation of clinopyroxene + spinel and amphibole + spinel symplectites in coronitic gabbros from the Sierra de San Luis (Argentina): a key to post-magmatic evolution. J Metamorph Geol 26:759–774

Deer WA, Howie RA, Zussman J (1966) An introduction to the rock-forming minerals. Longman Scientific & Technical Publishing, London

Deer WA, Howie RA, Zussman J (1992) An introduction to the rock-forming minerals. Longman Scientific & Technical Publishing, London

Dorfler KM, Tracy RJ, Caddick MJ (2014) Late-stage orogenic loading revealed by contact metamorphism in the northern Applachians, New York. J Metamorph Petrol 32:113–132

Duyverma HJ (1984) Late Precambrian granitic and volcanic rocks and their relation to cratonization of the Arabian Shield. Fac Earth Sci Bull 6:50–69

Efimov AA, Malitch KN (2012) Magnetite-orthopyroxene symplectites in gabbros of the Urals: a structural track of olivine oxidation. Geol Ore Deposits 54:531–539

El-Mettwaly A (1992) Pan-African post-orogenic gabbro cumulates from Sinai massif, Egypt: geochemistry and mineral chemistry. J Afr Earth Sci 14:217–225

Eyal M, Litvinovsky B, Jahn BM, Zanvilevich A, Katzir Y (2010) Origin and evolution of post-collisional magmatism: coeval Neoproterozoic calc-alkaline and alkaline suites of the Sinai Peninsula. Chem Geol 269:153–179

Farier GM (1985) Geological map of the Wadi Baysh quadrangle, Sheet 17 F, Saudi Arabia. Saudi Arabian Deputy Ministry for Mineral Resources, Geoscience Map GM-77, Scale 1:250,000, with explanatory notes

Fleck RJ, Greenwood WR, Hadley DG, Anderson RE, Schmidt DL (1980) Rubidium–Strontium geochronology and plate-tectonic evolution of the southern part of the Arabian Shield. Geological Survey Professional Paper 1131

Foster MD (1962) Interpretation of the composition and a classification of the chlorites. US Geological Survey Professional Paper 414A

Fritz H, Abdelsalam M, Ali KA, Bingen B, Collins AS, Fowler AR, Ghebreab W, Hauzenberger CA, Johnson PR, Kusky TM, Macey P, Muhongo S, Stern RJ, Viola G (2013) Orogen styles in the East African Orogen: a review of the Neoproterozoic to Cambrian tectonic evolution. J Afr Earth Sci 86:65–106

Gass IG (1981) Pan-African (upper Proterozoic) plate tectonics of the Arabian-Nubian Shield. In: Kröner A (ed) Precambrian plate tectonics. Developments in Precambrian geology 4, 1st edn. Elsevier, Amsterdam, pp 387–405

Genna A, Guerrot C, Deschamps Y, Nehlig P, Shanti M (1999) Les formations Ablah d'Arabie Saoudite (datation et implication géologique). Compte Rendu Acad Sci Paris 329:661–667

Genna A, Nehlig P, Le Goff E, Guerrot C, Shanti M (2002) Proterozoic tectonism of the Arabian Shield. Precambrian Res 117:21–40

Ghoneim MF (1988) Mineral chemistry of some gabbroic rocks of the central Eastern Desert, Egypt. Chem Erde 48:191–201

Giret A, Bonin B, Leger JM (1980) Amphibole compositional trends in oversaturated and undersaturated, alkaline plutonic ring complexes. Can Mineral 18:481–495

Golubkova AB, Nosova AA, Larionov YO (2014) Mg_ilmenite megacrysts from the Arkhangelsk kimberlites, Russia: genesis and Interaction with kimberlite melt and postkimberlite fluid. Geochem Int 51:353–381

Greenwood WR (1972) Geology of Al-Aqiq Quadrangle, South Saudi Arabia. Saudi Arabian Deputy Ministry for Mineral Resources, a geologic map with explanatory notes

Greiling RO, Abdeen MM, Dardir AA, El Akhal H, El-Ramly MF, Kamal El-Din GM, Osman AF, Rashwan AA, Rice AHN, Sadek MF (1994) A structural synthesis of the Proterozoic Arabian–Nubian Shield in Egypt. Geol Rundsch 83:484–501

Griffin WL (1971) Genesis of coronas in anorthosites of the Upper Jotun nappe, Indre Sogn, Norway. J Petrol 12:219–243

Gualda GAR, Vlach SRF (2005) Stoichiometry-based estimates of ferric iron in calcic, sodic-calcic and sodic amphiboles: a comparison of various methods. Anais da Academia Brasileira de Ciências 77:521–534

Hadley DG, Fleck RJ (1980) Reconnaissance geology of the Al Lith quadrangle, Sheet 24/40 C, Kingdom of Saudi Arabia. US Geological Survey Open-File Report 80-128

Haggerty SE (1976) Opaque mineral oxides in igneous rocks. In: Rumble D III (ed) Oxide minerals short course notes, vol 3. The Mineralogical Society of America, pp Hg-1–Hg-98

Haggerty SE, Tompkins LA (1984) Subsolidus reactions in kimberlitic ilmenites: exsolution, reduction and the redox state of the mantle. In: Kornprobst J (ed) Kimberlites 1: kimberlites and Related Rocks. Elsevier, Amsterdam, pp 83–105

Haggerty SE, Moore AE, Erlank AJ (1985) Macrocryst Fe–Ti oxides in olivine melilitites from Namaqualand–Bushmanland, South Africa. Contrib Mineral Petrol 91:163–170

Hamimi Z, El-Shafei M, Kattu G, Matsah M (2013) Transpressional regime in southern Arabian Shield: insights from Wadi Yiba Area, Saudi Arabia. Mineral Petrol 107:849–860

Hamimi Z, El-Fakharani A, Abdeen MM (2014) Polyphase deformation history and strain analyses of the post-amalgamation depositional basins in the Arabian–Nubian Shield: evidence from Fatima, Ablah and Hammamat basins. J Afr Earth Sc 99:64–92

Harris NB, Gass IG, Hawkesworth CJ (1990) A geochemical approach to allochthonous terranes: a Pan-African case study. Phil Trans Royal Soc London 331:533–548

Helmy HM, El-Mahallawi MM (2003) Gabbro Akarem mafic–ultramafic complex, Eastern Desert, Egypt: a Late Precambrian analogue of Alaskan-type complexes. Mineral Petrol 77:85–108

Helmy MH, Yoshikawa M, Shibata T, Arai S, Tamura A (2008) Corona structure from arc mafic–ultramafic cumulates: the role and chemical characteristics of late-magmatic hydrous liquids. J Mineral Petrol Sci 103:333–344

Helmy HM, Abd El-Rahman YM, Yoshikawa M, Shibata T, Arai S, Tamura A, Kagami H (2014) Petrology and Sm–Nd dating of the Genina Gharbia Alaskan-type complex (Egypt): insights into deep levels of Neoproterozoic island arcs. Lithos 198–199:263–280

Helmy HM, Yoshikawa M, Shibata T, Arai S, Kagami H (2015) Sm–Nd and Rb–Sr isotope geochemistry and petrology of Abu Hamamid intrusion, Eastern Desert, Egypt: an Alaskan-type complex in a back-arc setting. Precambrian Res 258:234–246

Helz RT (1973) Phase relations of basalts and their melting ranges at $P_{H_2O} = 5$ kb as a function of oxygen fugacity, part I: mafic phases. J Petrol 14:249–302

Henry DJ, Guidotti CV, Thomson JA (2005) The Ti-saturation surface for low to medium pressure metapelitic biotite: implications for geothermometry and Ti-substitution mechanisms. Am Mineral 90:316–328

Holland TJB, Blundy JD (1994) Non-ideal interactions in calcic amphiboles and their bearing an amphibole-plagioclase thermometry. Contrib Mineral Petrol 116:433–447

Inoue A, Meunier A, Partier-Mas P, Rigualt C, Beaufort D, Vieillard P (2009) Application of chemical geothermometry to low-grade temperature trioctahedral chlorites. Clays Clay Miner 57:371–382

Inoue A, Kurokawa K, Hatta T (2010) Application of chlorite geothermometry to hydrothermal alteration in Toyoha Geothermal System, southwestern Hokkaido, Japan. Res Geol 60:52–70

Irvine TN, Baragar WRA (1971) A guide to the chemical classification of the common volcanic rocks. Can J Earth Sci 8:523–548

Jarrar G, Stern RJ, Saffarini G, Al-Zubi H (2003) Late- and post-orogenic Neoproterozoic intrusions of Jordan: implications for crustal growth in the northernmost segment of the East African Orogen. Precambrian Res 123:295–319

Johnson PR (2003) Post-amalgamation basins of the NE Arabian Shield and implications for Neoproterozoic tectonism in the northern East African Orogen. Precambrian Res 123:321–337

Johnson PR (2006) Explanatory Notes to the Map of Proterozoic Geology of Western Saudi Arabia. Saudi Geological Survey Technical Report SGS-TR-2006-4, Scale 1:1,500,000, with explanatory notes

Johnson PR, Woldehaimanot B (2003) Development of the Arabian–Nubian Shield: perspectives on accretion and deformation in the northern East African Orogen and assembly of Gondwana. In: Yoshida M,Windley BF, Dasgupta S (eds) Proterozoic East Gondwana: supercontinent assembly and breakup. Geological Society Special Publications 206, pp 289–326

Johnson PR, Kattan FH, Wooden JL (2001) Implications of SHRIMP and microstructural data on the age and kinematics of shearing in the Asir Terrane, southern Arabian shield, Saudi Arabia. Gondwana Res 4:172–173

Johnson PR, Andresen A, Collins AS, Fowler AR, Fritz H, Ghebreab W, Kusky T, Stern RJ (2011) Late Cryogenian–Ediacaran history of the Arabian–Nubian Shield: a review of depositional, plutonic, structural, and tectonic events in the closing stages of the northern East African Orogen. J Afr Earth Sci 61:167–232

Johnson PR, Halverson GP, Kusky T, Stern RJ, Pease V (2013) Volcanosedimentary basins in the Arabian–Nubian Shield: markers of repeated exhumation and denudation in a Neoproterozoic accretionary orogen. Geosciences 3:389–445

Jowett EC (1991) Fitting iron and magnesium into hydrothermal chlorite geothermometer. GAC/MAC/SEG Joint Annual Meeting, Toronto, Program with Abstracts 16, A62

Kemp J, Pellaton C, Calvez JY (1980) Geochronological investigations and geological history in the Precambrian of northwestern Saudi Arabia. Saudi Arabian Directorate General of Mineral Resources Open-File Report BRGM-OF-01-1

Kemp J, Gros Y, Prian J-P (1982) Geologic map of the Mahd adh Dhahab quadrangle, sheet 23E, Kingdom of Saudi Arabia. Saudi Arabian Deputy Ministry for Mineral Resources Geologic Map GM 64, scale 1:250,000

Khalil AES, Obeid MA, Azer MK (2015) Late Neoproterozoic post-collisional mafic magmatism in the Arabian–Nubian Shield: a case study from Wadi El-Mahash gabbroic intrusion in southeast Sinai, Egypt. J Afr Earth Sci 105:29–46

Kranidiotis P, MacLean WH (1987) Systematics of chlorite alteration in the Phelps Dodge massive sulfide deposit, Matagami, Quebec. Econ Geol 82:1898–1911

Kröner A (1985) Ophiolites and the evolution boundaries in the late Proterozoic Arabian–Nubian Shield of Northeast Africa and Arabia. Precambrian Res 27:277–300

Laird J (1988) Chlorites: metamorphic petrology. In: Bailey SW (ed) Hydrous phyllosilicates (exclusive of micas), vol 19. The Mineralogical Society of America, pp 405–53

Leake BE, Woolley AR, Arps CES, Birch WD, Gilbert MC, Grice JD, Hawthorne FC, Kato A, Kisch HJ, Krivovichev VG, Linthout K, Laird J, Mandarino JA, Maresch WV, Nickel EH, Rock NMS, Schumacher JC, Smith DC, Stephenson NCN, Ungaretti L, Whittaker EJW, Youzhi G (1997) Nomenclature of amphiboles: report of the Subcommittee on Amphiboles of the International Mineralogical Association, Commission on New Minerals and Mineral Names. Am Mineral 82:1019–1037

Mehdilo A, Irannajad M (2010) Applied mineralogical studies on Iranian hard rock titanium deposit. J Miner Mater Character Eng 9:347–362

Miyashiro A (1975) Classification, characteristics and origin of ophiolites. J Geol 83:249–281

Mohamed FH, Hassanen MA (1996) Geochemical evolution of arc-related mafic plutonism district, Eastern Desert of Egypt in the Umm Nagat district, Eastern Desert of Egypt. J Afr Earth Sci 22:269–283

Morag N, Avigad D, Gerdes A, Belousova E, Harlavan Y (2011) Crustal evolution and recycling in the northern Arabian–Nubian Shield: new perspectives from zircon Lu–Hf and U–Pb systematic. Precambrian Res 186:101–116

Morimoto N, Fabries J, Ferguson AK, Ginzburg IV, Ross M, Seifert FA, Zussman J, Aoki K, Gottardi G (1988) Nomenclature of pyroxenes. Am Mineral 73:1123–1133

Morishita T, Arai S, Gervilla F (2001) High-pressure aluminous mafic rocks from the Ronda peridotite massif, southern Spain: significance of sapphirine- and corundum-bearing mineral assemblages. Lithos 57:143–161

Moufti MRH (2001) Age, geochemistry and origin of peraluminous A-type granitoids of the Ablah-Shuwas pluton, Ablah Graben Arabian Shield. Acta Mineral Petrogr 42:5–20

Nachit H, Razafimahefa N, Stussi J-M, Carron J-P (1985) Composition chimique des biotites et typologie magmatique des granitoïdes. Comp Rendus Acad Sci Series IIA Earth Planet Sci 301:813–818

Nachit H, Ibhi A, Abia E, Ben Ohoud M (2005) Discrimination entre biotites magmatiques primaires, biotites rééquilibrées et biotites néoformées. Compt Rendus Geosci Paris 337:1415–1420

Nehlig P, Salpeteur I, Asfirane F, Bouchot V, Eberle JM, Genna A, Kluyver HM, Lasserre JL, Nicol N, Recoche G, Shanti M, Thieblemont D, Tourliere B (1999) The Mineral Potential of the Arabian Shield: a re-assessment. UGS/UNESCO Meeting on the Base and Precious Metal Deposits in the Arabian Shield, Jeddah, pp 12–19

Nehlig P, Genna A, Asfirane F (2002) A review of the Pan-African evolution of the Arabian Shield. GeoArabia 7:103–124

Nimis P, Taylor WR (2000) Single clinopyroxene thermobarometry for garnet peridotites. Part I. Calibration and testing of a Cr-in-cpx barometer and an enstatite-in-cpx thermometer. Contrib Mineral Petrol 139:541–554

Parsapoor A, Khalili M, Tepley F, Maghami M (2014) Mineral chemistry and isotopic composition of magmatic, re-equilibrated and hydrothermal biotites from Darreh-Zar porphyry copper deposit, Kerman (Southeast of Iran). Ore Geol Rev 66:200–218

Patino Douce AE (1993) Titanium substitution in biotite: an empirical model with applications to thermometry, O_2 and H_2O barometers, and consequence for biotite stability. Chem Geol 108:132–162

Putirka KD (2008) Thermometers and barometers for volcanic systems. Rev Mineral Geochem 69:61–120

Qaoud N, Abdelnasser A (2012) Geochemistry and petrogenesis of El-Fringa meragabbro-diorite rocks, Wadi Sa'al area, south Sinai, Egypt. J Al Azhar Univ Gaza Nat Sci 14:111–138

René M (2011) Titanite-ilmenite assemblage in microgranodiorites from the northeastern margin of the Klenov granite body (Bohenian Massif, Czech Republic). Acta Geodyn Geomater 8:479–487

Rossi P, Chévremont P (1987) Classification des associations magmatiques granitoïdes. Geochronique 21:14–18

Sasaki K, Nakashima K, Kanisawa S (2003) Pyrophanite and high Mn ilmenite discovered in the Cretaceous Tono pluton, NE Japan. Neues Jahrb Mineral Monats 2003:302–320

Saunders AD, Tarney J, Weaver SD (1980) Transverse geochemical variations across the Antarctic Peninsula: implications for the genesis of calc-alkaline magmas. Earth Planet Sci Lett 46:344–360

Spencer KJ, Lindsley DH (1981) A solution model for coexisting iron–titanium oxides. Am Mineral 66:1189–1201

Stern RJ (1994) Arc assembly and continental collision in the Neoproterozoic East-African Orogen-implications for the consolidation of Gondwana land. Annu Rev Earth Planet Sci 22:319–351

Stern RJ, Johnson PR (2010) Continental lithosphere of the Arabian Plate: a geologic, petrologic, and geophysical synthesis. Earth Sci Rev 101:29–67

Sun SS, McDonough WF (1989) Chemical and isotopic systematic of ocean basalts: implication for mantle composition and processes. In: Saunders AD, Norry MJ (eds), Magmatism in the ocean basins. Geological Society London Special Publications 42, pp 313–345

Taj RJ, Mesaed AA (2011) Depositional and diagenetic history of the Neoproterozoic silicified stromatolitic carbonates, west of Wadi Girshah, Ablah district, western Arabian Shield, Saudi Arabia. Int J Sci Eng Res 2:1–18

Tarassova E, Tarassov M, Tacheva E, Nedialkov R (2009) Indicative properties of accessory magnetite and ilmenite from mixed magma of Petrohan pluton, Western Balkan, Bulgaria. In: Proceedings of annual science conference Bulgarian Geological Society, Sofia, Bulgaria, 3–4 Dec 2009, pp 13–14

Turner SP, Stüwe K (1992) Low-pressure corona textures between olivine and plagioclase in unmetamorphosed gabbros from Black Hill, South Australia. Mineral Mag 56:503–509

Velde B (1985) Clay minerals: a physico-chemical explanation of their occurrence. Elsevier, Amsterdam

Velde B, Medhioub M (1988) Approach to chemical equilibrium in diagenetic chlorites. Contrib Mineral Petrol 98:122–127

Velde B, El Moutaouakkil N, Iijima A (1991) Compositional homogeneity in low-temperature chlorites. Contrib Mineral Petrol 107:21–26

Vernon RH (2004) A practical guide to rock microstructure. Cambridge University Press, Cambridge, UK

Vidal O, Parra T, Vieillard P (2005) Thermodynamic properties of the Tschermak solid solution in Fe-chlorite: application to natural examples and possible role of oxidation. Am Mineral 90:347–358

Vidal O, De Andrade V, Lewin E, Munoz M, Parra T, Pascarelli S (2006) P–T-deformation-Fe^{3+}/Fe^{+} mapping at the thin section scale and comparison with XANES mapping: application to a garnet-bearing metapelite from the Sambagawa metamorphic belt (Japan). J Metamorph Geol 24:669–683

Wier KL, Hadley DG (1975) Reconnaissance geology of the Wadi Sa'diyah quadrangle, Sheet 20/40 A, Kingdom of Saudi Arabia. US Geol Surv Open-File Report 75-493

Wiewiora A, Weiss Z (1990) Crystallochemical classifications of phyllosilicates based on the unified system of projection of chemical composition: II. The chlorite group. Clay Miner 25:83–92

Wilde SA, Youssef K (2002) A re-evaluation of the origin and setting of the Late Precambrian Hammamat Group based on SHRIMP U-Pb dating of detrital zircons from Gebel Umm Tawat, North Eastern Desert, Egypt. J Geol Soc London 159:595–604

Wilson M (1989) Igneous petrogenesis. Unwin Hyman, London

Yau Y-C, Peacor DR, Beane RE, Essene EJ, McDowell SD (1988) Microstructures, formation mechanisms and depth-zoning of phyllosilicates in geothermally altered shales, Salton Sea, CA. Clays Clay Miner 36:1–10

Zakir FA (1972) Geology of the Ablah area, Southern Hijaz Quadrangle, Kingdom of Saudi Arabia. Dissertation, South Dakota School of Mines and Technology, Rapid City, USA

Zane A, Weiss Z (1998) A procedure for classifying rock-forming chlorites based on microprobe data. Rendiconti Lincei 9:51–56